Optimization of Placement and Resource Allocation in UAV-aided Multi-hop Wireless Networks

Mohammadsaleh Nikooroo, Omid Esrafilian, Zdenek Becvar, David Gesbert

***Abstract*—This paper investigates the performance of cellular networks assisted by unmanned aerial vehicles (UAVs) acting as flying base stations (FlyBSs). We focus on a scenario with multi-hop relaying via FlyBSs to deliver data from a ground base station (GBS) to users in a challenging case with the channels reused at all hops to exploit radio resources efficiently. Our objective is to maximize the sum capacity of the users via an optimization of FlyBSs' position in 3D, association of users to either GBS or to one of the FlyBSs, allocation of channels for communication at individual hops, and allocation of transmission power for all channels. Moreover, practical constraints on the FlyBSs' movement, transmission and propulsion power, and backhaul capacity are taken into account. Due to a non-convexity and discreetness of the objective and some constraints, there is no optimal solution to the formulated problem. Thus, we propose an analytical solution based on an alternating optimization of an energy-efficient placement of the FlyBSs, channel allocation, user association, and transmission power. Each subproblem in the alternating optimization is substituted either by a linear programming (LP) problem through a change of variables, or by a convex problem via a conversion of the objective and constraints. The results show an increase in sum capacity by 35%–60% compared to related works while the FlyBSs' propulsion power consumption is not increased.**

***Index Terms*—Flying base station, multi-hop relaying, wireless backhaul, channel reuse, sum capacity, mobile networks, 6G.**

I. Introduction

Deployment of unmanned aerial vehicles (UAVs) as flying base stations (FlyBSs) has been investigated heavily in the past years. Intrinsic characteristics, such as mobility and adaptability to the users requirements and environment makes the FlyBSs an efficient tool to deliver high quality of services to users via improved channels gain, enhancement of line of sight (LoS) probability, reduced transmission power consumption, extension of coverage, etc. [1], [51], [3]. An improvement in the system performance via the FlyBSs is reached provided that several aspects, including a placement of FlyBSs, energy consumption, and resource management [4], [5], [6] are carefully addressed. These aspect are even more pronounced in the scenario with multiple FlyBSs due to mutual interference among them [7]. The mutual interference can be mitigated by orthogonal resources allocated for individual FlyBSs. However, the usage orthogonal radio resources with no reuse leads to a low spectral efficiency. In contrast, the reuse of resources usually results in intricate and complex problem to be solved due to non-convex objective and/or constraints.

The situation becomes even more complicated if relaying via multiple FlyBSs (multi-hop) is supported to improve performance. The basic version of relaying is a two-hop model that considers FlyBSs placed at the access link, i.e., the FlyBSs serve the users directly and relay data between a ground base station (GBS) and the users [8], [9]. Several recent works study the two-hop relaying networks with *single* FlyBS from a perspective of an analysis of the coverage/outage probability [10], [11], sum capacity maximization [12], [13], [14], optimization of required number of FlyBSs [15], minimization of FlyBS's propulsion power [16], or minimization of network latency [17]. Nevertheless, an extension of these works designed for single FlyBS to multiple-FlyBS scenario is not trivial.

The two-hop relaying with *multiple* FlyBSs is also considered in literature for optimization of, e.g., ratio of covered users to energy consumption [18], network's utility [19], network latency [20], sum capacity [21], [22], [23], minimum throughput of all links [24], minimum user's rate [25], or aggregated energy efficiency [26]. Even if multiple FlyBSs are considered, the two-hop relaying might not be efficient if the channel conditions between the FlyBSs and the GBS are poor due to obstacles, or distance. An extension of the two-hop relaying to higher number of hops is often not possible or straightforward due to the constraints introduced by backhaul capacity at individual hops.

There are only a limited number of works that consider more than two hops for relaying via FlyBSs. In [27], resource allocation and FlyBS's positioning are studied in the network with a single FlyBS connected to the network via a satellite serving the ground users. In [28], the problem of joint optimization of transmission power and FlyBSs' placement is investigated to maximize the throughput between two users. The solution in [28], however, only assumes a horizontal placement of the FlyBSs. Furthermore, an association of users to individual relays is not addressed. In [29], the authors minimize the transmission energy consumption of relaying FlyBSs to establish a time-slotted communication between source and destination nodes. Nevertheless, the aspects of FlyBS's positioning, user association, and channel allocation are not addressed. In [30], the problem of optimization of the number of FlyBSs and 2D positioning of relaying FlyBSs is investigated to ensure a certain required level of signal-to-noise ratio (SNR) among

Mohammadsaleh Nikooroo and Zdenek Becvar are with the Department of Telecommunication Engineering, Faculty of Electrical Engineering, Czech Technical University in Prague, Czech Republic, e-mail: (nikoomoh@fel.cvut.cz and zdenek.becvar@fel.cvut.cz). Omid Esrafilian and David Gesbert are with the Communication Systems Department, EURECOM, Sophia Antipolis, France, e-mail: (esrafili@eurecom.fr and gesbert@eurecom.fr).

This work was supported by the project No. LTT 20004 funded by Ministry of Education, Youth and Sports, Czech Republic and by the grant of Czech Technical University in Prague No. SGS23/171/OHK3/3T/13, and partially by the HUAWEI France supported Chair on Future Wireless Networks at EURECOM.

the FlyBSs. The aspects of backhaul constraints, transmission power allocation, and channel allocation are, however, not addressed. In [31], the problem of relaying FlyBS's positioning and transmission power allocation is studied to minimize a utility function that is defined as a weighted summation of the FlyBSs' altitude and transmission power. Still, the backhaul connectivity, user association, and channel allocation are not addressed. Then, in [32], the authors consider a multi-hop relaying in a scenario where multiple small cells are connected to a core network through a set of FlyBSs. Each small cell is served by one FlyBS, and the FlyBSs are connected to the core network via another relaying FlyBS. The total sum rate of the small cells is maximized via a positioning of the FlyBSs and association of small cells to the FlyBSs at the access link. In [33], the authors minimize the cost of FlyBSs' deployment via FlyBSs' positioning and resource allocation to ensure quality of service to the users. The authors consider scenario with three hops, but with only one FlyBS at the first hop for relaying data between the GBS and other FlyBSs. The problem of FlyBSs' placement is investigated in [34] to minimize the communication delay for users. The provided solutions in [33] and [34], however, assume orthogonal transmission. On one hand, interference among FlyBSs is not present making the problem easier to solve. On the other hand, radio resources are not used efficiently and, thus, performance is limited. In [35], the number of FlyBSs required for a multi-hop relaying is investigated to ensure coverage of the users while still guaranteeing connectivity of the FlyBSs to the GBS through backhaul. Furthermore, the authors in [36] deploy multi-hop FlyBSs to connect remote users to the GBS and propose an interference management scheme based on machine learning and a positioning based on K-means to maximize energy efficiency.

In our prior work [37], the sum capacity is maximized via the FlyBS's positioning and transmission power allocation at the access link, but the backhaul is neglected.

In our another work [38], the transmission power is optimized over the backhaul channels with a channel reuse for single FlyBS in a two-hop network. Furthermore, we also study the problem of user association and FlyBSs' positioning in the scenario with multi-hop relaying with a single relaying FlyBS in [9].

In the view of the conducted research on relaying via FlyBSs as explained above, an inclusion of *multiple relaying FlyBSs* in a *multi-hop* scenario together with the aspects of *user association*, *channel allocation*, *3D positioning of the FlyBSs*, and *transmission power allocation* over all *GBS-FlyBS*, *GBS-user*, *FlyBS-FlyBS*, and *FlyBS-user* channels is not yet addressed in literature. The optimization of all the mentioned aspects is not addressed even for a simple two-hop relaying via FlyBSs in existing literature while we address it in multi-hop scenario. Hence, we provide a framework to address all the aforementioned key aspects in the scenarios with multiple FlyBSs serving mobile users. The proposed work goes even beyond addressing those aspects by also enabling a multi-hop relaying across the FlyBSs and allowing the GBS and all FlyBSs in multi-hop scenario to serve users directly, which is also not considered in the related works and it changes the derived solution significantly. Due to interference resulting from channel reuse, multiple FlyBSs, and multi-hop communication, the existing solutions dealing with non-convexity of similar objectives/constraints cannot be applied.

The main contributions of this paper are further elaborated as follow

- We formulate the problem of sum capacity maximization via an optimization of 3D placement of FlyBSs, user association, channel allocation, and transmission power allocation in the networks moving users in multi-hop scenario. Besides, to increase an efficiency of the radio resource usage, a full channel reuse at all hops is allowed and practical constraints, such as FlyBSs' altitude, maximum flying speed, transmission and propulsion energy consumption, and maximum transmission power are considered. Moreover, the relaying causality is taken into account.
- Due to a discreetness of certain variables and non-convexity of the objective and some constraints, the formulated problem cannot be solved optimally. Hence, we propose an iterative, but quickly converging solution based on an alternating optimization of all variables. For the user association and channel allocation, a change of variables is proposed to convert the problem to a linear programming (LP) problem. Furthermore, the FlyBSs' placement and the transmission power allocation are both solved via proposed iterative approaches. For each derived subproblem, analytical solutions are proposed and developed to deal with the non-convexity of the objective functions and constraints in a way that the sequence of those steps leads to a converging solution without a violation of the constraints in the problem.
- We demonstrate that our proposed solution increases the sum capacity by 35%–60% compared to state-of-the-art works while the total energy consumption, consisting of transmission and propulsion, is close to these state-of-the-art schemes.

The rest of this paper is organized as follows. The system model for multi-hop relaying is presented in Section II. Then, the problem of sum capacity maximization under practical constraints is formulated in Section III. In Section IV, the proposed methodology to solve the formulated problem is outlined, and the challenges related to solving the problem are explained. Next, Section V demonstrates our proposed solution to the FlyBSs' positioning. In Section VI, the problem of joint optimization of the channel allocation and the user association is targeted. Then, in Section VII, the problem of the transmission power allocation to the channels is investigated. Next, the overall proposed solution is summarized with its computational complexity discussed in Section VIII. Then, we explain the simulation scenario in Section VIII and we present the results to benchmark the performance of the proposed solution against the state of the art. Last, Section IX concludes the work and suggests further advancements for the future.

II. System model

In this section, we outline the scenario and network model and we explain the model adopted for system parameters such

as user association, transmission channels as well as channel allocation, and transmission power. Then, we formulate user's capacity. The key notations used throughout the paper is listed in Table I.

Notation: for a clarity of presentation of notations used throughout the paper, scalar parameters are shown by a plain *italic* font, whereas vectors are shown by **boldface** font, and sets are presented by *calligraphic* font.

A. Scenario and network model

We consider a set of M FlyBSs providing coverage to a set of N mobile users $\mathcal{U} = \{u_1, ..., u_N\}$. The FlyBSs are connected to the GBS either directly or via other relaying FlyBSs. For a clarity of presentation, the FlyBSs that only serve the users and not another FlyBS(s) are referred to as the *access* FlyBSs, or FlyBSs at the *access link* throughout the rest of this paper. Then, the term *relaying* FlyBSs is used for the FlyBSs that facilitate the backhaul communication for other FlyBSs (in addition to serving the users directly). Let $\mathcal{M}_{\mathcal{R}}$ and $\mathcal{M}_{\mathcal{A}}$ denote the set of indices for the relaying FlyBSs and the access FlyBSs, respectively. The FlyBSs in both tiers $\mathcal{M}_{\mathcal{R}}$ and $\mathcal{M}_{\mathcal{A}}$ as well as the GBS can serve the users directly. Following the defined notations, $\mathcal{M} = \mathcal{M}_{\mathcal{R}} \cup \mathcal{M}_{\mathcal{A}} \cup \{0\}$ is the set of indices of all BSs including GBS and FlyBSs, where the index zero represents the GBS. Without loss of generality, we assume that $\mathcal{M}_{\mathcal{A}} = [1, M_a]$ and $\mathcal{M}_{\mathcal{R}} = [M_a + 1, M_a + M_r]$. Hence, $|\mathcal{M}| = M + 1 = M_a + M_r + 1$. Each of the access FlyBSs can potentially communicate with all the relaying FlyBSs simultaneously. Fig. 1 depicts the connection between the BSs and the users as well as the connection among the BSs.

Let $\boldsymbol{Q} = \{\boldsymbol{q_0}, ..., \boldsymbol{q_M}\}$ be the set of locations of all BSs, where $\boldsymbol{q_m}[t] = \big[X_m[t], Y_m[t], H_m[t]\big]^T$ is the location of the BS m $(0 \leq m \leq M)$. The location of the user n at the time step k is denoted by $\boldsymbol{q_n}[t] = \big[x_n[t], y_n[t], z_n[t]\big]^T$. Furthermore, let $d_{m,m'}[t]$ and $d_{n,m}[t]$ denote the Euclidean distance between the BSs m' and m and between the user n and the BS m, respectively.

Note that the duration of each time step, denoted by δ_t, is chosen to be small enough so that the FlyBS's displacement can be modeled as a constant velocity motion [14], [50]. The speed of the FlyBS m at the time step t is denoted by $V_m[t]$ an calculated as

$$V_m[t] = \frac{1}{\delta_t} ||\boldsymbol{q_m}[t] - \boldsymbol{q_m}[t-1]||, \tag{1}$$

where $||.||$ is the $\mathcal{L}^2$ norm.

B. User association and channel allocation

The association of users to any BSs is represented by a binary matrix $\boldsymbol{A} = (a_{n,m}) \in \{0,1\}^{N \times (M+1)}$ such that, for columns $\{0, \ldots, M\}$ in $\boldsymbol{A}$, $a_{n,m} = 1$ indicates the user n being served by the BS m and $a_{n,m} = 0$ otherwise. Note that the column "0" indicates the GBS. As in common cases, each user is served by just one BS at any time step, i.e.,

$$\sum_{m \in \mathcal{M}} a_{n,m}[t] \leq 1, \quad \forall n, \quad a_{n,m}[t] \in \{0,1\} \tag{2}$$

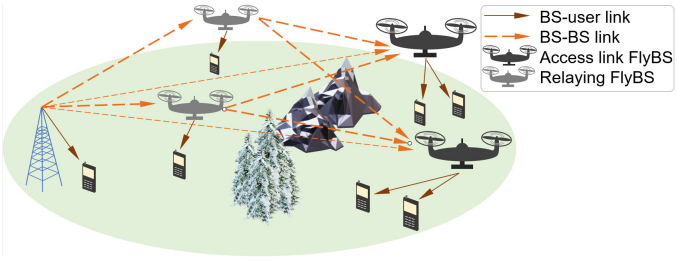

Figure 1: Multi-hop model with access FlyBSs, relaying FlyBSs, and GBS serving moving users. Each BS-user or BS-BS link can comprise none, one, or multiple channels. A user can be served by any BS. The interference at the users/BSs caused by other BSs (due to channel reuse) is not shown to avoid cluttering.

Now let us explain the channel allocation. Assume that $\chi = \{\chi_1, \ldots, \chi_K\}$ is the set of available channels (sub-bands) so that the channels are orthogonal to each other. Then, let B_k denote the bandwidth of χ_k $(k \in [1, K])$. We model the channel allocation as a mapping

$$\boldsymbol{I} : \chi \rightarrow \{\cup_{m,m' \in \mathcal{M}}(m, m'), \cup_{m \in \mathcal{M}, n \in [1,N]}(m, n)\}, \tag{3}$$

where each channel (indexed within $[1, K]$) is allocated for the transmission between the BS m and the BS m' $(m \neq m')$ and/or between the BS m and the user n.

Also, let I_m be the set of indices of channels used by the BS m to transmit. Furthermore, for a clearer presentation of formulations, let $I_{m,m'} \subseteq I_m$ denote the set of channels used by the BS m to transmit to the BS m'. Fig. 2 demonstrates the adopted channel allocation. The blocks on the left-hand side represent the channels to be assigned to the GBS-FlyBS, GBS-user, FlyBS-FlyBS, and FlyBS-user links on the right-hand side.

Note that in this paper, parameters related to channels are sometimes formulated at the user's end. Hence, we also adopt the specific notation $\boldsymbol{k_n}$ to indicate the index set of channels allocated to the user n.

In our system model, we assume that each BS uses orthogonal channels to transmit to different BSs/users. Nevertheless, different BSs can use same channels. Since the number of channels allocated to $|I_m|$ and $|I_{m,m'}|$ for all m and m' cannot exceed the total number of available channels, we have

$$|I_m| \leq K, \quad |I_{m,m'}| \leq K. \quad \forall m, m' \in \mathcal{M} \tag{4}$$

Furthermore, we assume full-duplex FlyBSs. Hence, such full-duplex operation incurs self-interference at each FlyBS's transmitter over same channels used for both receiving and transmitting.

C. Propulsion power and transmission power consumption

The propulsion power consumption is modeled in line with [39] for quad-rotor UAVs. In particular, the propulsion power consumption of the FlyBS m is denoted as $P_{pr,m}$ and calculated in terms of the FlyBS's speed V_m as follows

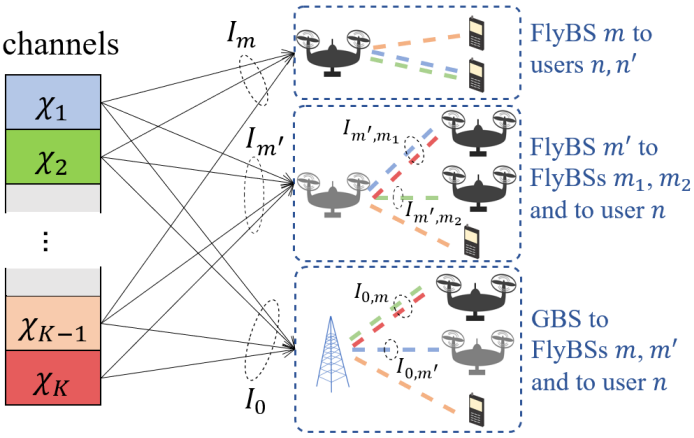

Figure 2: Illustration of channel allocation model. Each channel is represented by a block on the left hand side and is mapped to the BS-BS or the BS-user link.

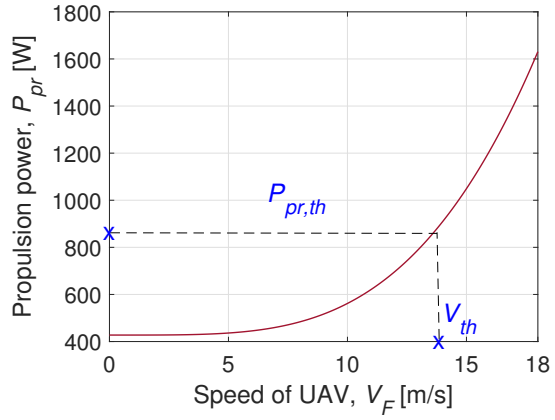

Figure 3: Propulsion power consumption versus flying speed for quad-rotor UAVs. A maximum threshold of $P_{pr,th}$ for propulsion power consumption corresponds to a maximum flying speed of V_{th}.

$$P_{pr,m} = \frac{c_4}{4}\left(\frac{\beta^2 g^2}{\vartheta_t^2} + \frac{\vartheta_d^2}{\vartheta_t^2} V_m^4\right) + \frac{c_3}{2}\left(\frac{\beta^2 g^2}{\vartheta_t^2} + \frac{\vartheta_d^2}{\vartheta_t^2} V_m^4\right)^{\frac{3}{4}} + c_2\left(\frac{\beta^2 g^2}{\vartheta_t^2} + \frac{\vartheta_d^2}{\vartheta_t^2} V_m^4\right)^{\frac{1}{2}} + 2c_1\left(\frac{\beta^2 g^2}{\vartheta_t^2} + \frac{\vartheta_d^2}{\vartheta_t^2} V_m^4\right)^{\frac{1}{4}} + 4c_0, \quad (5)$$

where β is the FlyBS's mass, g is the acceleration of gravity, ϑ_d is the fuselage drag ratio, ϑ_t is the thrust coefficient, and the coefficients c_0, c_1, c_2, c_3, c_4 are defined as

$$c_0 = \phi_0^2 R_0, c_1 = 30\Omega_E \frac{\phi_0}{\pi}, c_2 = 2\Upsilon R_0 \frac{\phi_0}{\Omega_T}, \quad c_3 = 30\Upsilon \frac{\Omega_E}{(\pi\Omega_T)}, c_4 = \Upsilon^2 \frac{R_0}{\Omega_T^2}, \quad (6)$$

where the parameters ϕ_0, R_0, Ω_E, Υ, and Ω_T are the FlyBS's no-load current, motor resistance, back-electromotive force constant, torque coefficient, and torque constant, respectively. Fig. 3 demonstrates the propulsion power consumption versus the FlyBS's speed (V_m).

The transmission power, let $\boldsymbol{P} = (p_{k,m}^{TX})$ be a K-by-$(M+1)$ matrix, where $p_{k,m}^{TX}$ denotes the transmission power of the BS m over the channel k. The power $p_{n,m,k}^{R}$ received by the user n over the channel k ($k \in \boldsymbol{k_n}$) is then calculated as:

$$p_{n,m,k}^{R} = \kappa_{n,m,k}[t] d_{n,m}^{-\alpha_{n,m}}[t] p_{k,m}^{TX}[t], \quad (7)$$

with $\kappa_{n,m,k} \stackrel{\text{def}}{=} \Gamma_{n,m}(\frac{\gamma}{\gamma+1}\overline{h}_n + \frac{1}{\gamma+1}\tilde{h}_n) d_{n,m}^{-\alpha_{n,m}} p_{k,m}^{TX}$, where the parameter $\Gamma_{n,m}$ depends on communication frequency and gain of antennas, γ is the Rician fading factor, $\overline{h}_n$ is the line-of-sight (LoS) complex component satisfying $|\overline{h}_n| = 1$, $\tilde{h}_n$ denotes the non-line-of-sight (NLoS) complex component satisfying $\tilde{h}_n \sim CN(0,1)$, and $\alpha_{n,m}$ is the pathloss exponent.

A similar relation applies for the transmission and received power over backhaul link, i.e.,:

$$p_{m,m',k}^{R}[t] = \kappa_{m,m',k} d_{m,m'}^{-\alpha_{m,m'}}[t] p_{k,m'}^{TX}[t], \quad (8)$$

where $p_{m,m',k}^{R}$ is the received signal power at the BS m from the BS m' over the channel k.

D. Communication capacity formulation

The downlink capacity of the user n over the channel s is denoted by $C_{n,m,k}$ and is calculated as

$$C_{n,m,k}[t] = B_k \log_2\left(1 + \frac{p_{n,m,k}^{R}[t]}{\sigma_{n,k}^2 + \sum_{m' \in \{a_{n,m'}=0\}} p_{n,m',k}^{R}[t]}\right), \quad (9)$$

where $\sigma_{n,k}^2$ is the noise power over the assigned channel k at the link to the user n.

Then, the overall capacity of the user n from the BS m is denoted by $C_{n,m}$ and defined as

$$C_{n,m}[t] = \sum_{k \in \boldsymbol{k_n}} B_s \log_2\left(1 + \frac{p_{n,m,k}^{R}[t]}{\sigma_{n,k}^2 + \sum_{m' \in \{a_{n,m'}=0\}} p_{n,m',k}^{R}[t]}\right), \quad (10)$$

Next, for the access FlyBS m, the capacity from the BS m' ($m' \in \mathcal{M}_{\mathcal{R}} \cup \{0\}$) is denoted as $C_{m,m'}$ and calculated as follow

$$C_{m,m'}[t] = \sum_{k \in I_{m,m'}} B_k \times \quad (11)$$
$$\log_2\left(1 + \frac{p_{m,m',k}^{R}[t]}{\sigma_{m,k}^2 + g_{k,m}^{SI} p_{k,m}^{TX}[t] + \sum_{m'' \in \mathcal{M}_{\mathcal{R}} \cup \{0\} - \{m'\}} p_{m,m'',k}^{R}[t]}\right),$$

where $g_{k,m}^{SI}$ is the gain of the channel k due to the m-th FlyBS's self-interference [21], [40].

The capacity of the relaying FlyBS m' ($m' \in \mathcal{M}_{\mathcal{R}}$) from the GBS is

$$C_{m',0}[t] = \quad (12)$$
$$\sum_{k \in I_{m',0}} B_k \log_2\left(1 + \frac{p_{m',0,k}^{R}[t]}{\sigma_{m',k}^2 + g_{k,m'}^{SI} p_{k,m'}^{TX}[t] + \sum_{m'' \in \mathcal{M}_{\mathcal{R}}} p_{m',m'',k}^{R}[t]}\right).$$

III. Problem Formulation

In this section, we introduce the problem of sum capacity maximization and we explain the challenges regarding the solution to user association, channel allocation, transmission power allocation, and FlyBS's positioning.

Our goal is to maximize the sum capacity at every time step t via associating the users to the BSs (including GBS and FlyBSs), allocating channels and transmission power to the BSs, and 3D positioning of the FlyBSs. The problem is formulated

Table I: KEY NOTATIONS ADOPTED IN THIS PAPER

Notation	Description
$\mathcal{M}$, M	set of all BSs including GBS, total number of BSs
$\mathcal{U}$, N, u_n	set of users, number of users, user n
$\mathcal{M}_{\mathcal{R}}$, M_r	set of relaying FlyBSs, number of relaying FlyBSs
$\mathcal{M}_{\mathcal{A}}$, M_a	set of access FlyBSs, number of access FlyBSs
$\boldsymbol{Q}$, $\boldsymbol{q_m}$, $\boldsymbol{q_n}$	position of all BSs, position of BS m, position of user n
$[x_n, y_n, z_n]$	x, y, and z coordinates of user n
$[X_m, Y_m, H_m]$	x, y, and z coordinates of BS m
$H_{m,min}$, $H_{m,max}$	minimum altitude of FlyBS m, maximum altitude of FlyBS m
V_m, $V_{m,max}$	speed of FlyBS m, maximum speed limit of FlyBS m
t, δ_t	index used for time step, duration of time step t
$P_{pr,m}$, $P_{pr,m,th}$	propulsion power of FlyBS m, threshold of propulsion power
$d_{m,m'}$, $d_{m,n}$	distance between BSs, distance between BS and user
$\boldsymbol{A}$, $a_{n,m}$	association matrix, binary association indicator of user n to BS m
$C_{n,m}$, $C_{m,m'}$	capacity at user n from BS m, capacity at BS m from BS m'
$\boldsymbol{k_n}$, k	index set of channels allocated to u_n, general channel index
K	total number of channels
χ, χ_k, B_k	set of all channels, channel k, bandwidth of channel k
$\boldsymbol{I}$	channel allocation mapping for BS-user and BS-BS links
$e_{k,m,m'}$, $e_{k,m,n}$	binary indicators of channel allocation to BS-BS and BS-user links
I_m, $I_{m,m'}$	channels used by BS m, channels used in BS-BS links
ι_{max}	maximum number of channels assigned to each BS-user channel
$\boldsymbol{P}$	transmission power vector over all channels
$p^{TX}_{k,m}$, $p^{TX}_{m,max}$	TX power of BS m over channel k, maximum TX power of BS m
$p^{R}_{n,m,k}$	signal power received by user n from BS m over channel s
$p^{R}_{m,m',k}$	signal power received by BS m from BS m' over channel s
$\kappa_{n,m,k}$	coefficient fulfilling $p^{R}_{n,m,k} = \kappa_{n,m,k} d^{-\alpha_{n,m}}_{n,m} p^{TX}_{k,m}$
$\kappa_{m,m',k}$	coefficient fulfilling $p^{R}_{m,m',k} = \kappa_{m,m',k} d^{-\alpha_{m,m'}}_{m,m'} p^{TX}_{k,m'}$
$g^{SI}_{k,m}$	channel gain for self interference of BS m over channel k

under constraints on the FlyBSs' altitude, speed, maximum transmission power, and propulsion power threshold, as well as constraints on the backhaul links. Hence, we formulate the problem of the sum capacity maximization as follows

$$\mathbf{P1}: \max_{\boldsymbol{I},\boldsymbol{P},\boldsymbol{A},\boldsymbol{Q}} \sum_{m\in\mathcal{M}} \sum_{n=1}^{N} a_{n,m} C_{n,m}[t],\ \forall k \tag{13}$$

$$\text{s.t.} \quad H_{m,min} \le H_m[t] \le H_{m,max}, \tag{13a}$$

$$V_m[t] \le V_{max}, \quad m \in [1, M_a + M_r] \tag{13b}$$

$$\sum_{n=1}^{N} a_{n,m} C_{n,m}[t] \le \sum_{m'\in\mathcal{M}_{\mathcal{R}}} C_{m,m'}[t], \quad m \in \mathcal{M}_{\mathcal{A}} \tag{13c}$$

$$\sum_{n=1}^{N} a_{n,m'} C_{n,m'}[t] + \sum_{m\in\mathcal{M}_{\mathcal{A}}} C_{m',m}[t] \le C_{0,m'}[t], m' \in \mathcal{M}_{\mathcal{R}} \tag{13d}$$

$$\sum_{k=1}^{K} p^{TX}_{k,m}[t] \le p^{TX}_{m,max}, \quad p^{TX}_{k,m}[t] \ge 0, \quad m \in \mathcal{M} \tag{13e}$$

$$P_{pr,m}[t] \le P_{pr,m,th}[t], \quad m \in \mathcal{M}_{\mathcal{R}} \cup \mathcal{M}_{\mathcal{A}} \tag{13f}$$

$$(2), (4),$$

where $H_{m,min}$ and $H_{m,max}$ in (13a) limit the minimum and maximum flying altitudes of the FlyBS m, respectively. Furthermore, V_{max} in (13b) is the maximum supported speed of FlyBSs. In addition, (13c) ensures that the capacity over the backhaul link for each access FlyBS is not lower than the FlyBS's sum downlink capacity, and the constraint (13d) suggests that the link capacity between the GBS and each relaying FlyBS is not lower than the total capacity that the relaying FlyBS provides to the users and to the access FlyBSs. The constraint (13e) indicates that the transmitting power for each BS should not exceed the maximum transmission power of the BS. Furthermore, the constraint (13f) limits the propulsion power consumption of the FlyBS m to the maximum value of $P_{pr,th,m}$ and this maximum value is set arbitrarily so that the positioning of FlyBSs does not incur excessive energy consumption, which would potentially affect the FlyBS's performance adversely. In general, $P_{pr,th,m}$ can be dynamically adjusted over time and according to the FlyBSs' available energy to maintain the FlyBS's operation. A setting of such upper bound $P_{pr,th,m}$ is introduced in, e.g., [46] to prolong the FlyBS's coverage.

Challenges regarding the optimization problem P1 in (13) include: 1) the sum capacity function is non-concave with respect to the FlyBSs' positions (i.e., $\boldsymbol{q_m}$, $m \in \mathcal{M}_{\mathcal{R}} \cup \mathcal{M}_{\mathcal{A}}$) as well as to the transmission power $\boldsymbol{P}$, 2) the backhaul constraints (13c) and (13d) are non-convex with respect to the FlyBSs' positions ($\boldsymbol{Q}$) and transmission power ($\boldsymbol{P}$), and 3) the discrete user association $\boldsymbol{A}$ and channel allocation $\boldsymbol{I}$ makes the optimization problem (13) non-tractable. Due to the challenges above, only sub-optimal solutions can be provided. To tackle these challenges, we propose a heuristic solution to (13) by the means of alternating optimization of all four variables in P1. Still, the alternating optimization of the variables (as explained later) faces complications (due to non-convexity) with the optimal derivation of either of the target variables. Hence, several tricks and analytical transformations are proposed.

Note that, in contrast to some existing works targeting the aggregated sum capacity over multiple time-slots, we choose the instantaneous sum capacity as the objective in P1. This is due to the fact that the maximization of the aggregated sum capacity is not feasible in scenarios (including ours) where the knowledge of the future locations of the users is naturally unavailable. In such scenarios, the optimization of the sum capacity at every time step is a reasonable approach. This is justified by stressing the fact that, despite an unpredictable future of the users' locations, the users' displacements are still constrained by their limited moving speed, and the optimization time step can be set to a short duration (say, a second). Hence, the next optimal positions of the FlyBSs (to which the FlyBSs move to in the next time step) are typically close to their optimal positions from the previous time step. It is worth mentioning that, the unavailable future knowledge of the network parameters is the only factor keeping us from optimizing the aggregated sum capacity. Otherwise, the challenges to deal with the hypothetical objective and the constraints are quite similar to those mentioned above regarding solving P1. In particular, the hypothetical objective is a summation of the objective in P1 over multiple time steps, and once the objective in P1 is converted to a convex or to an LP problem via our proposed solution (as will be explained in the following sections), the hypothetical objective could use the same procedure at every time step to convert to a convex or to an LP problem, respectively. Furthermore, all the constraints in P1 still apply for each time step of the hypothetical problem.

In the following section, we outline our proposed solution.

IV. OVERVIEW OF THE PROPOSED SOLUTION

In this section, we outline principle of the proposed solution to the problem P1. To solve the problem P1, we propose an

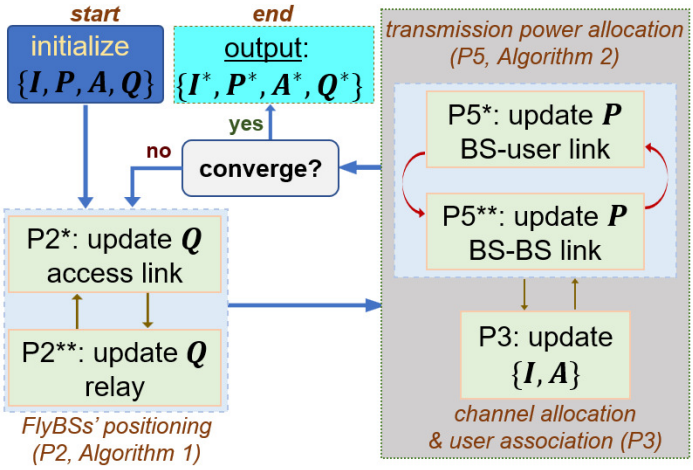

Figure 4: Schematic of the solution based on alternating optimization of the variables $\boldsymbol{I}$, $\boldsymbol{P}$, $\boldsymbol{A}$, and $\boldsymbol{Q}$ with the converged outcome $\{\boldsymbol{I}^*, \boldsymbol{P}^*, \boldsymbol{A}^*, \boldsymbol{Q}^*\}$.

alternating optimization of the variables, since a derivation of the optimal solution to the non-convex problem in P1 is not possible. Our solution is inspired by the basic approach of alternating optimization although with specific modifications in line with the nature of the optimization variables.

Fig. 4 depicts the flow of the proposed alternating optimization. At the beginning, the variables $\{\boldsymbol{I}, \boldsymbol{P}, \boldsymbol{A}, \boldsymbol{Q}\}$ are initialized by the values of these variables derived for the previous time step. For $t = 1$, the initialization is done by picking random values that fulfill the constraints in (13). Next, the position of the FlyBSs $\boldsymbol{Q}$ are updated while the values of the other optimization variables are temporarily fixed. This task itself is split into two steps: i) positioning of the access FlyBSs, and ii) positioning of the relaying FlyBSs. These two steps are iterated until convergence. Then, a joint optimization of the discrete variables $\{\boldsymbol{I}, \boldsymbol{A}\}$ is targeted while the values of other variables are fixed. Afterwards, the transmission power allocation $\boldsymbol{P}$ is optimized at a fixed setting of the other variables. To this end, the transmission power is optimized by iteratively updating the transmission power over BS-user links and BS-BS links until convergence. Now, although an optimization of all variables is performed once, we do not yet consider the first round of optimization as completed. More specifically, there is a relatively greater impact of the variables $\boldsymbol{P}$ and $\{\boldsymbol{I}, \boldsymbol{A}\}$ on each other compared to $\boldsymbol{Q}$. Hence, the latest update of $\boldsymbol{P}$ is intuitively more suitable to be followed by a further update of $\{\boldsymbol{I}, \boldsymbol{A}\}$ rather than an update of $\boldsymbol{Q}$. This is shown in Fig. 4 as an iterative process inside of the gray block. Of course, once the interchanging update of $\boldsymbol{P}$ and $\{\boldsymbol{I}, \boldsymbol{A}\}$ converges, the next round of optimization starts by an update of $\boldsymbol{Q}$, and so on, unless a new round is not required due to a convergence of all variables.

The reason for updating each of the variables $\boldsymbol{Q}$ and $\boldsymbol{P}$ in two steps relates to our proposed methodology. More specifically, if the approximations used to tackle the non-concavity of objective or the non-convexity of constraints are applied in separate steps, they would perform better and with lower approximation error compared to the case where the approximations are applied all at once. This proposed approach is elaborated in the next sections.

Furthermore, note that the reason for selecting the order of optimizations as it is explained above (and shown in Fig. 4) is due to a relaxation of some constraints. More specifically, in the course of updating each of the target variables, some constraints may be relaxed in order to facilitate a solution. However, despite such local relaxations, the proposed sequence of optimization will still ensure that the final solution fulfills all the constraints included in P1. Moreover, the solution converges at every round (iteration) of optimization with only a polynomial computational complexity. As we show later via simulations, the entire proposed solution converges in only a few iterations.

V. FlyBS Placement

As the first part of the proposed alternating optimization, we provide the positioning of the FlyBSs with respect to a fixed setting of $\boldsymbol{I}$, $\boldsymbol{P}$, and $\boldsymbol{A}$. To this end, we first modify the problem P1 and we explain the proposed solution consisting of placement of the the access FlyBSs and the relaying FlyBSs, as described in the following subsections.

A. Formulation of the FlyBS placement problem

The subproblem of the FlyBSs' placement with respect to constraints from (13) related to positioning (i.e., (13a),(13b),(13c),(13d),(13f)) is formulated as follow

$$\mathbf{P2}: \max_{\boldsymbol{Q}} \sum_{m\in\mathcal{M}} \sum_{n=1}^{N} a_{n,m} C_{n,m}[t], \ \forall k$$

$$\text{s.t.} \quad (13a), (13b), (13c), (13d), (13f), \tag{14}$$

The constraints (13a), (13b), and (13f) are convex with respect to $\boldsymbol{Q}$, however, the objective (sum capacity) is neither convex nor concave, and the constraints (13c) and (13d) are not convex. To address these challenges, we propose a substitution of the objective and the constraints to convert P2 to a convex problem. In particular, we replace the objective with a concave under-estimator, and the constraints (13c) and (13d) with convex constraints such that, upon a fulfillment of the alternative constraints, the original constraints are met as well. Note that, after the convex alternative problem to P2 is solved, the convex approximation process is repeated with the approximations in the new round done with respect to the optimal $\boldsymbol{Q}$ derived from the previous round so that the process results in an increasing converging values for the objective in P2.

Moreover, the approximation to convert P2 to a convex problem would require several steps if the positions of both relaying and access FlyBSs' are targeted simultaneously, which overcomplicates the solution and also leads to redundant errors in approximation. Hence, we propose a solution based on an alternating optimization of the relaying and access FlyBSs. To this end, assuming a fixed position of the relaying FlyBSs, the position of the access FlyBS m ($m \in \mathcal{M}_{\mathcal{A}}$) is updated and, then, the position of the relaying FlyBS m' ($m' \in \mathcal{M}_{\mathcal{R}}$) is optimized for the fixed (updated) positions of the access FlyBSs. In the following, we elaborate the proposed solution.

B. FlyBS placement at the access link

Following the discussion earlier in this section, the problem of access FlyBSs' positioning at the is first formulated for a given fixed position of the relaying FlyBSs as follow

$$\textbf{P2*}: \max_{\boldsymbol{q_{m'}}} \sum_{m\in\mathcal{M}}\sum_{n=1}^{N} a_{n,m}C_{n,m}[t],\ m'\in\mathcal{M}_{\mathcal{A}}, \forall k$$

$$\text{s.t.} \quad (13a), (13b), (13c), (13d), (13f), \tag{15}$$

The objective in P2* is non-concave and the constraints (13c) and (13d) are non-convex with respect to $\boldsymbol{q_{m'}}$, $m'\in\mathcal{M}_{\mathcal{A}}$. In the following Proposition 1, we propose a solution to deal with P2*.

Proposition 1. *The problem in P2* can be converted to a convex problem without a violation of the constraints as explained in Appendix A.*

Proof. See Appendix A. □

C. Placement of relaying FlyBSs

Once the placement of the access FlyBSs is carried out according to the proposed solution presented in Section V.B, the relaying FlyBSs are then positioned. Thus, the subproblem of relaying FlyBS positioning is formulated as

$$\textbf{P2**}: \max_{\boldsymbol{q_{m'}}} \sum_{m\in\mathcal{M}}\sum_{n=1}^{N} a_{n,m}C_{n,m}[t],\ m'\in\mathcal{M}_{\mathcal{R}}, \forall k \tag{16}$$

$$\text{s.t.} \quad (13a), (13b), (13c), (13d), (13f).$$

Similarly as in P2*, the objective is neither concave nor convex with respect to the optimization variable, i.e., the relaying FlyBSs' positions q_m ($m\in\mathcal{M}_{\mathcal{R}}$). Furthermore, the constraints (13c) and (13d) are also non-convex. Hence, in the following, we propose a solution to tackle the non-convexity.

Proposition 2. *The problem in P2** can be converted to a convex problem without a violation of the constraints as explained in Appendix B.*

Proof. See Appendix B. □

Algorithm 1 demonstrates the proposed solution to FlyBSs positioning. According to the lines 3-9, the positions of the access FlyBSs are derived via approximating P2* with a convex problem, solving it, and repeatedly updating it using derived values from previous iteration. Once converged, the subproblem of the relaying FlyBS positioning is then solved via converting P2** to a convex problem and iteratively updating it with respect to the optimal values derived in the previous iteration. In case the FlyBSs are not converged, the explained two-step process is repeated until convergence.

After the positioning of the FlyBSs, the optimization of the variables $\boldsymbol{I}$, $\boldsymbol{P}$, and $\boldsymbol{A}$ (as will be explained later) is repeated until convergence, that is, until there is no further change in the outcome of any of the variables $\boldsymbol{I}$, $\boldsymbol{P}$, $\boldsymbol{A}$, and $\boldsymbol{Q}$.

Algorithm 1 FlyBS positioning

$\boldsymbol{q_{m,(0)}}$: initialized positions of BSs
$\boldsymbol{\lambda}_{k,m}$: auxiliary variable to track convergence for $\boldsymbol{q_m}$
$\{\boldsymbol{A}, \boldsymbol{I}, \boldsymbol{P}\}$: preset user association, channel allocation, and transmission power of BSs

1: $\boldsymbol{\lambda}_{k,m} \leftarrow \boldsymbol{q_{m,(0)}}$
2: **repeat**
3: **repeat**
4: substitute the objective in P2* at $\boldsymbol{q_{m,(0)}}$ according to (30)-(33)
5: substitute (13c) with a convex constraint by applying (35)-(38) at $\boldsymbol{q_{m,(0)}}$ for $\{\boldsymbol{A}, \boldsymbol{I}, \boldsymbol{P}\}$
6: apply (39)-(42) at $\boldsymbol{q_{m,(0)}}$ and at $\{\boldsymbol{A}, \boldsymbol{I}, \boldsymbol{P}\}$ to replace (13d) with a convex constraint
7: modify P2* according to lines 4-6 and solve using CVX
8: update $\boldsymbol{q_{m,(0)}}$ according to solution in line 7
9: **until** convergence of $\boldsymbol{\lambda}_{k,m}$
10: **repeat**
11: substitute the objective in P2** at $\boldsymbol{q_{m,(0)}}$ according to (43)
12: derive a convex constraint from (13c) by applying (45) at $\boldsymbol{q_{m,(0)}}$ for $\{\boldsymbol{A}, \boldsymbol{I}, \boldsymbol{P}\}$
13: derive a convex constraint from (13d) by applying (46)-(48) at $\boldsymbol{q_{m,(0)}}$ for $\{\boldsymbol{A}, \boldsymbol{I}, \boldsymbol{P}\}$
14: solve P2** with the updated constraints in lines 11-13 using CVX
15: update $\boldsymbol{q_{m,(0)}}$ according to solution in line 14
16: **until** convergence of $\boldsymbol{\lambda}_{k,m}$
17: $\boldsymbol{\lambda}_{k,m} \leftarrow \boldsymbol{q_{m,(0)}}$
18: **until** convergence of $\boldsymbol{\lambda}_{k,m}$

Output: position of the BSs $\boldsymbol{q_m}$, $m\in\mathcal{M}$.

VI. Channel allocation and User association

In this section, we demonstrate our solution to the user association and the channel allocation. We propose to determine the variables $\boldsymbol{I}$ and $\boldsymbol{A}$ jointly. In other words, each channel is assigned to the user-BS and BS-BS links. Of course, this joint optimization is done with respect to the constraints (2) and (4). To this end, we first formulate the subproblem of user association and channel allocation as

$$\textbf{P3}: \max_{\boldsymbol{I},\boldsymbol{A}} \sum_{m\in\mathcal{M}}\sum_{n=1}^{N} a_{n,m}C_{n,m}[t],\ \forall k \tag{17}$$

$$\text{s.t.} \quad (2), (4), (13c), (13d).$$

The backhaul constraints (13c) and (13d) complicate the solution due to a discrete nature of $\boldsymbol{I}$ and $\boldsymbol{A}$. Nevertheless, neglecting these constraints would normally lead to solutions to P3, where the channels are chiefly assigned to BS-user links, and consequently, the backhaul link would become the bottleneck limiting the sum capacity. In order to tackle this issue, we temper the formulated problem in P3 by the following steps: i) (13c) and (13d) are relaxed and are directly taken into account when optimizing the placement of the FlyBSs (Section V) and the transmission power (later in Section VII), and ii) in order to not limit the backhaul capacity, we define an

auxiliary condition such that the number of assigned channels to any BS-user link should not exceed an arbitrarily set value of ι_{max}. We further elaborate this condition and the way of setting it later in this section.

A. Reformulation of P3

Following the explained adjustments above, we propose a conversion of P3 to an LP problem. This is done using a definition of new auxiliary variables. In particular, we set the binary parameter $e_{k,m,m'}[t]$ such that $e_{k,m,m'}[t] = 1$ indicates the channel χ_k being assigned to the link between the BSs m and m' at the time t, and $e_{k,m,m'}[t] = 0$ otherwise. Similar definition is made for $e_{k,m,n}$ (for instance, in Fig. 2, the parameters $e_{K-1,m,n}$, $e_{2,m,n'}$, e_{1,m',m_1}, $e_{K-1,0,n}$ are all equal to one). The value of $e_{k,m,n}$ can be determined via a knowledge of values of both $\boldsymbol{k_n}$ and $a_{n,m}$, and vice versa. To begin with a conversion of P3 according to the newly defined variable $e_{k,m,n}$, we first re-express the defined auxiliary condition on the maximum number of assigned channels to each BS-user link (as mentioned earlier in this section) as

$$\sum_{k\in K}\sum_{m\in\mathcal{M}} e_{k,m,n} \leq \iota_{max},\ \forall n \tag{18}$$

Next, the assumption of orthogonality among the channels used by same BS to transmit to other BSs/users is formulated as

$$e_{k,m,m'}[t]e_{k,m,i}[t] = 0,\ \ m' \neq i \tag{19}$$
$$e_{k,m,i} \in \{0,1\},\ \ m \in \mathcal{M}_{\mathcal{R}} \cup \{0\},\ m', i \in \mathcal{M}_{\mathcal{A}} \cup [1,N],$$

where

$$e_{k,m,i} \in \{0,1\},\ \ m \in \mathcal{M}_{\mathcal{R}} \cup \{0\}, i \in \mathcal{M}_{\mathcal{A}} \cup [1,N]. \tag{20}$$

According to (19) and (20), $e_{k,m,m'}$ and $e_{k,m,i}$ cannot be equal to one at the same time, meaning that each BS m maintains orthogonal transmissions to other BSs/users. Note that this condition, straightforward as it sounds, is quadratic. In order to reduce the complexity of the problem and its solution, we use the fact that $e_{k,m,i}$ ($i \in \mathcal{M}_{\mathcal{A}} \cup [1,N]$) is a binary variable. Using this fact, we convert (19) to a linear equivalent constraint

$$\sum_{i\in\mathcal{M}_{\mathcal{A}}\cup[1,N]} e_{k,m,i} \leq 1, m \in \mathcal{M}_{\mathcal{R}} \cup \{0\}. \tag{21}$$

Next, in order to formulate the sum capacity in terms of $e_{k,m,n}$, we point to the fact that, if $a_{n,m} = 0$, then $e_{k,m,n} = 0$ for any channel k. Furthermore, if $a_{n,m} = 1$ (i.e., the user n is associated to the BS m), then the capacity of the user n is calculated by summing over all channels assigned to the link between the user n and the BS m, or in other words, over channels fulfilling $e_{k,m,n} = 1$. Hence, the objective in P3 is rewritten as

$$\sum_{n=1}^{N} a_{n,m}C_{n,m}[t] = \sum_{k\in[1,K]}\sum_{m\in\mathcal{M}}\sum_{n=1}^{N} e_{k,m,n}C_{n,m}[t], \tag{22}$$

Furthermore, the constraint (2) is rewritten in terms of $e_{k,m,n}$ as

$$\sum_{m\in\mathcal{M}} e_{k,m,n} \leq 1,\ \forall n \tag{23}$$

Also, the constraint (4) is rewritten as

$$\sum_{k\in[1,K]}\sum_{n=1}^{N} e_{k,m,n} \leq K,\ m \in \mathcal{M}_{\mathcal{R}} \cup \{0\},$$
$$\sum_{m'\in\mathcal{M}_{\mathcal{A}}}\sum_{k\in[1,K]} e_{k,m,m'} \leq K,\ m \in \mathcal{M}_{\mathcal{R}} \cup \{0\}. \tag{24}$$

With the conversion of the objective and associated constraints as explained above, the problem in P3 is converted to maximization of sum capacity in (22) via a determination of $e_{k,m,i}$ and under the constraints (21), (23), and (24) as follows

$$\textbf{P4}: \max_{e_{k,m,i}} \sum_{k\in[1,K]}\sum_{m\in\mathcal{M}}\sum_{n=1}^{N} e_{k,m,n}C_{n,m}[t],\ i \in \mathcal{M}_{\mathcal{A}} \cup [1,N] \tag{25}$$
$$\text{s.t.}\quad (18), (20), (21), (23), (24).$$

Solving P4 is challenging due to the binary nature of $e_{k,m,i}$. To tackle this, we first relax the binary constraint (20) and solve the following relaxed problem

$$\textbf{P4*}: \max_{e_{k,m,i}} \sum_{k\in[1,K]}\sum_{m\in\mathcal{M}}\sum_{n=1}^{N} e_{k,m,n}C_{n,m}[t],\ i \in \mathcal{M}_{\mathcal{A}} \cup [1,N] \tag{26}$$
$$\text{s.t.}\quad (18), (21), (23), (24).$$

According to P4*, the objective in P4* as well as the constraints (18), (21), (23), and (24) are linear with respect to $e_{k,m,n}$. Hence, P4* is an LP problem, and we solve it using the interior-point method in *linprog* tool in MATLAB. Next, the solution to P4 is calculated via rounding the values of $e_{k,m,i}$ derived from the solution to P4*.

Last, the following Proposition provides the setting of ι_{max} in (18).

Proposition 3. *To solve P4*, the value of ι_{max} in (18) is derived as explained in Appendix C.*

Proof. See Appendix C. □

VII. Transmission power allocation

In this section, we focus on the allocation of the transmission power over FlyBS-user channels as well as over the backhaul. Before providing the solution for transmission power allocation, we formulate the problem to be solved considering the general defined problem P1.

A. Formulation of power allocation problem

Note that, although the transmissions over the backhaul links are considered as interference in the sum capacity (according to (10)), decreasing the transmission power on the backhaul channels would not necessarily increase the user capacity, since decreasing the backhaul transmission power

would lower the backhaul capacity, which would result in limiting the achieved capacity of the users. Thus, we formulate the subproblem of transmission power allocation while keeping backhaul constraints (13c) and (13d) as follows

$$\mathbf{P5}: \max_{\boldsymbol{P}} \sum_{m\in\mathcal{M}} \sum_{n=1}^{N} a_{n,m} C_{n,m}[t],\ \forall t \tag{27}$$

$$\text{s.t.} \quad (13c), (13d), (13e).$$

Challenges regarding solution to P5 are that the objective is neither convex nor concave with respect to the power vector $\boldsymbol{P}$, and the constraints (13c) and (13d) are also non-convex. To tackle these challenges, convex substitutions of the objective as well as the constraints in P5 are proposed. To this end, certain approximations are applied. The approximations are proposed in a way such that i) the alternative (convex) objective is set to be an under-estimator of the original objective in P5 so that the maximization of the alternative objective would result in enhancement of the original objective, and ii) the derived alternative (convex) constraints would be no looser than the original constraints, hence, a fulfillment of the alternative constraints would automatically fulfills the original constraints.

Before elaborating the solution according to steps i and ii above, we note that the process of convex approximation of P5 is of an iterative manner. More specifically, the process in the steps i and ii leads to a convergent solution to the alternative problem to P5. In order to fully exploit the mentioned optimization technique, after the alternative problem to P5 is solved, the steps i and ii are repeated such that the approximation in the new round is done using the derived (optimal) values for $\boldsymbol{P}$ from the previous round. This way, not only the derived optimal value to the alternative objective increases in every iteration, but it converge eventually.

Now let us elaborate the steps i and ii. In the course of the approximations for the objective and the constraints in P5, the approximations used for the transmission power over BS-user channels does not conform well with the approximations over BS-BS links, in the sense that, applying both types of approximation to the same objective/constraint would either be very complicated, and/or result in excessive error in approximations. To avoid such unwanted complications, we propose a solution in two steps where the transmission power is first optimized over the BS-user links and, then, over the backhaul BS-BS links. In the following subsections, we elaborate our proposed solutions for both links.

B. Power allocation over BS-user links

In line with the approach explained earlier in this section, we formulate the subproblem of power allocation for BSs as follow

$$\mathbf{P5^*}: \max_{p^{TX}_{k,m}} \sum_{m\in\mathcal{M}} \sum_{n=1}^{N} a_{n,m} C_{n,m}[t],\ k \in I_m \tag{28}$$

$$\text{s.t.} \quad (13c), (13d), (13e).$$

The objective in P5* is non-concave and the constraints (13c) and (13d) are non-convex with respect to $p^{TX}_{k,m}$, $m \in \mathcal{M}$, $k \in I_m$. In the following Proposition 4, we propose a solution to convert P5* to convex.

Proposition 4. *The problem in P5* is solved by converting the problem to convex using approximations on the objective function and the constraints (13c) and (13d) as explained in Appendix D.*

Proof. See Appendix D. □

C. Power allocation over BS-BS links

After optimization of the transmission power over the BS-user links, the subproblem of transmission power optimization for the BS-BS links with respect to associated constraints is formulated as follows

$$\mathbf{P5^{**}}: \max_{p^{TX}_{k,m'}} \sum_{m\in\mathcal{M}} \sum_{n=1}^{N} a_{n,m} C_{n,m}[t],\ k \in I_{m,m'} \tag{29}$$

$$\text{s.t.} \quad (13c), (13d), (13e).$$

The objective in P5** is non-concave and the constraints (13c) and (13d) are non-convex with respect to $p^{TX}_{k,m'}$, $m' \in \mathcal{M} - \{m\}$, $k \in I_{m,m'}$. In the following Proposition 5, we propose a solution to tackle the mentioned non-concavity/-convexity.

Proposition 5. *The problem in P5** is solved by converting the problem to convex using approximations on the objective function and the constraints (13c) and (13d) as explained in Appendix E.*

Proof. See Appendix E. □

D. Algorithm for transmission power allocation

Algorithm 2 demonstrates the solution to P5. According to the lines 3-9 in Algorithm 2, the subproblem of transmission power allocation for the BS-user links is solved via iteratively converting the problem P5* into the convex problem with respect to the derived values from previous iteration. Next, the lines 10-15 provide a similar iterative solution via converting P5** to the convex problem using derived values from previous iteration. Then, in line 16, the transmission power is calculated and, in case not converged yet, the algorithm repeats the procedure.

VIII. Overall proposed algorithm for optimization of multi-hop relaying via FlyBSs

In this section, we sum up the steps towards an optimization of the user association, channel allocation, and transmission power allocation and FlyBSs' positioning as elaborated in the Sections V-VII and we discuss the computational complexity of the solution.

Algorithm 2 Transmission power allocation

$p^{TX}_{k,m,(0)}$, $m \in \mathcal{M}$, $k \in [1, K]$: initialized transmission power of BSs over channels
$\rho_{k,m}$: auxiliary variable to track convergence for $p^{TX}_{k,m}$
$\{\boldsymbol{A}, \boldsymbol{I}, \boldsymbol{Q}\}$: preset user association, channel allocation, and BSs' positions

1: $\rho_{k,m} \leftarrow p^{TX}_{k,m,(0)}$
2: **repeat**
3: **repeat**
4: substitute the objective in P5* at $p^{TX}_{k,m,(0)}$ according to (50)
5: substitute (13c) with a convex constraint by applying (51)-(55) at $p^{TX}_{k,m,(0)}$ for $\{\boldsymbol{A}, \boldsymbol{I}, \boldsymbol{Q}\}$
6: substitute (13d) with a convex constraint similarly as in line 5
7: modify P5* according to lines 4-6 and solve using CVX
8: update $p^{TX}_{k,m,(0)}$ according to solution in line 7
9: **until** convergence of $\rho_{k,m}$
10: **repeat**
11: derive a convex constraint from (13c) by applying (56) at $p^{TX}_{k,m,(0)}$ for $\{\boldsymbol{A}, \boldsymbol{I}, \boldsymbol{Q}\}$
12: derive a convex constraint from (13d) by applying (57)-(59) at $p^{TX}_{k,m,(0)}$ for $\{\boldsymbol{A}, \boldsymbol{I}, \boldsymbol{Q}\}$
13: use CVX to solve P5** with the updated constraints from lines 11-12
14: update $p^{TX}_{k,m,(0)}$ according to solution in line 13
15: **until** convergence of $\rho_{k,m}$
16: $\rho_{k,m} \leftarrow p^{TX}_{k,m,0}$
17: **until** convergence of $\rho_{k,m}$

Output: BSs' transmission power over channels $p^{TX}_{k,m}$, $m \in \mathcal{M}$, $k \in [1, K]$.

A. Overall proposed solution

Algorithm 3 shows the overall proposed solution to the original problem in P1 at one time step t. For every setting of ι_{max}, we use auxiliary variables $\mathrm{C_{tm}}$ and $\{\boldsymbol{A}_{\mathbf{0},\mathrm{tm}}, \boldsymbol{I}_{\mathbf{0},\mathrm{tm}}, \boldsymbol{P}_{\mathbf{0},\mathrm{tm}}, \boldsymbol{Q}_{\mathbf{0},\mathrm{tm}}\}$ to keep track of changes in values of sum capacity and $\{\boldsymbol{A}, \boldsymbol{I}, \boldsymbol{P}, \boldsymbol{Q}\}$, respectively. Furthermore, a binary variable ω is adopted such that $\omega = 1$ indicates that the algorithm has finally reached the optimal ι_{max}. According to Algorithm 3, the optimization variables, ι_{max}, ω, and $\mathrm{C_{tm}}$ are first initialized in the lines 1 and 2. Then, according to the proposed alternating optimization of the variables, the positioning $\boldsymbol{Q}$ is first optimized in line 6, and then, the optimization of $\boldsymbol{I}$, $\boldsymbol{A}$, and $\boldsymbol{P}$ is targeted (lines 8-13) at a fixed value for $\boldsymbol{Q}$ as derived previously. In particular, $\boldsymbol{I}$ and $\boldsymbol{A}$ are jointly optimized (line 9), and then $\boldsymbol{P}$ is updated (line 11) with respect to the updated values of $\boldsymbol{I}$ and $\boldsymbol{A}$. This interactive optimization continues until convergence of all of $\boldsymbol{I}$, $\boldsymbol{A}$, and $\boldsymbol{P}$. In case the sum capacity is not converged, the newly derived $\boldsymbol{I}$, $\boldsymbol{A}$, and $\boldsymbol{P}$ are used as preset values to repeat the next round of optimization with updating $\boldsymbol{Q}$ again, and so on. After convergence of the sum capacity, the current value of ι_{max} is decreased by one (line 16), and the same optimization procedure is repeated. The optimal value of ι_{max} is reached when the sum capacity starts decreasing by further lowering of ι_{max}. For the next time step, Algorithm 3 is repeated with the updated initial values of $\{\boldsymbol{A_0}, \boldsymbol{I_0}, \boldsymbol{P_0}, \boldsymbol{Q_0}\}$ using the result from its previous time step and according to line 18.

B. Complexity of the proposed solution

To calculate the computational complexity of the proposed solution to P2, we first note that there are M_r decision variables and $2M_r + 2M$ constraints in P2*, as well as M_a decision variables and $2M_a + 2M$ constraints in P2**. Hence, the complexities of P2* and P2** scale as $\mathcal{O}({M_r}^2(2M_r + 2M)^{2.5} + (2M_r + 2M)^{3.5})$ and $\mathcal{O}({M_a}^2(2M_a + 2M)^{2.5} + (2M_a + 2M)^{3.5})$, respectively. Hence, the overall complexity of the solution to P2 is $\mathcal{O}({M_r}^2(M_r + M)^{2.5} + (M_r + M)^{3.5} + {M_a}^2(M_a + M)^{2.5} + (M_a + M)^{3.5})$, or more simply as $\mathcal{O}({M_r}^{4.5}{M_a}^{2.5} + {M_r}^{2.5}{M_a}^{4.5})$. The derived complexity is deemed favorable as the typical values of M_r and M_a in practice are low (order of one). Note that the complexity corresponding to a conversion of the subproblems P2* and P2** are much less than the calculated complexities above, and are not mentioned here as they do not change the derived order of overall complexity.

Furthermore, the LP programming problem in P4 includes LP programming, for which a derivation of computational complexity is not conventional due to a relatively high dependency of the complexity on the objective as well as on a correlation between the variables which is represented by the set of constraints in the problem. Only upper bounds with worst-cases analyses have been provided in the literature for that matter [41], [42]. In the following, we derive an upper bound for complexity similarly as in [41]. In P4, there are $K(M_rM_a + (M_r + M_a)N)$ decision variables and $2N + 3M_r + 3$ constraints. Since the number of decision variables is higher than the number of constraints, then according to [41], the computational complexity of the interior-point method

Algorithm 3 User association, channel allocation, power allocation, and FlyBS positioning

ω: binary flag to indicate reaching optimal ι_{max}
$\mathrm{C_{tm}}$: temporary value of sum capacity
$\{\boldsymbol{A_0}, \boldsymbol{I_0}, \boldsymbol{P_0}, \boldsymbol{Q_0}\}$: initialized optimization variables
$\{\boldsymbol{A}_{\mathbf{0},\mathrm{tm}}, \boldsymbol{I}_{\mathbf{0},\mathrm{tm}}, \boldsymbol{P}_{\mathbf{0},\mathrm{tm}}, \boldsymbol{Q}_{\mathbf{0},\mathrm{tm}}\}$: temporary value of variables

1: $\{\boldsymbol{A}, \boldsymbol{I}, \boldsymbol{P}, \boldsymbol{Q}\} \leftarrow \{\boldsymbol{A_0}, \boldsymbol{I_0}, \boldsymbol{P_0}, \boldsymbol{Q_0}\}$
2: $\iota_{max} \leftarrow K$, $\omega \leftarrow 0$, $\mathrm{C_{tm}} \leftarrow 0$
3: **while** $\sim \omega$
4: $\{\boldsymbol{A}_{\mathbf{0},\mathrm{tm}}, \boldsymbol{I}_{\mathbf{0},\mathrm{tm}}, \boldsymbol{P}_{\mathbf{0},\mathrm{tm}}, \boldsymbol{Q}_{\mathbf{0},\mathrm{tm}}\} \leftarrow \{\boldsymbol{A_0}, \boldsymbol{I_0}, \boldsymbol{P_0}, \boldsymbol{Q_0}\}$
5: **repeat**
6: derive $\boldsymbol{Q}$ from P2 at $\boldsymbol{A}_{\mathbf{0},\mathrm{tm}}, \boldsymbol{I}_{\mathbf{0},\mathrm{tm}}, \boldsymbol{P}_{\mathbf{0},\mathrm{tm}}$ using Algorithm 1
7: $\boldsymbol{Q}_{\mathbf{0},\mathrm{tm}} \leftarrow \boldsymbol{Q}$
8: **repeat**
9: find $\boldsymbol{I}$ and $\boldsymbol{A}$ via solving the LP problem P4 at $\boldsymbol{P}_{\mathbf{0},\mathrm{tm}}$, $\boldsymbol{Q}_{\mathbf{0},\mathrm{tm}}$
10: $\boldsymbol{A}_{\mathbf{0},\mathrm{tm}} \leftarrow \boldsymbol{A}$, $\boldsymbol{I}_{\mathbf{0},\mathrm{tm}} \leftarrow \boldsymbol{I}$
11: solve P5 to find $\boldsymbol{P}$ at $\boldsymbol{A}_{\mathbf{0},\mathrm{tm}}$, $\boldsymbol{I}_{\mathbf{0},\mathrm{tm}}$, $\boldsymbol{Q}_{\mathbf{0},\mathrm{tm}}$ using Algorithm 2
12: $\boldsymbol{P}_{\mathbf{0},\mathrm{tm}} \leftarrow \boldsymbol{P}$
13: **until** convergence of $\boldsymbol{A}$, $\boldsymbol{I}$, $\boldsymbol{P}$
14: **until** convergence of sum capacity
15: **if** sum capacity increased, update $\mathrm{C_{tm}}$ **else** $\omega \leftarrow 1$ **End if**
16: $\iota_{max} \leftarrow \iota_{max} - 1$
17: **End while**
18: $\{\boldsymbol{A_0}, \boldsymbol{I_0}, \boldsymbol{P_0}, \boldsymbol{Q_0}\} \leftarrow \{\boldsymbol{A}_{\mathbf{0},\mathrm{tm}}, \boldsymbol{I}_{\mathbf{0},\mathrm{tm}}, \boldsymbol{P}_{\mathbf{0},\mathrm{tm}}, \boldsymbol{Q}_{\mathbf{0},\mathrm{tm}}\}$

Output:$\{\boldsymbol{A}, \boldsymbol{I}, \boldsymbol{P}, \boldsymbol{Q}\}$

is upper bounded by $\mathcal{O}\Big(\big(KM_rM_a + (M_r + M_a)N\big)^{3.5}\Big)$, or more simply by $\mathcal{O}\Big(K^{3.5}M^{3.5}N^{3.5}\Big)$ for each setting of ι_{max}. Then, since a determination of ι_{max} requires a repetition of the solution to P4 by at most K times, the overall complexity of solution to P3 is then upper bounded by $\mathcal{O}\Big(K^{4.5}M^{3.5}N^{3.5}\Big)$. Even though the actual computational complexity is supposed to be smaller, still the derived upper bound is of polynomial complexity and confirms that the proposed solution is suitable for a relatively wide range of M, K and N in practice.

Next, to calculate the complexity of the proposed solution to P5*, let us note that there are a maximum of $KN(M+1)$ decision variables in P5* (depending on the apriori channel allocation and user association) as well as $2M$ constraints. Hence, the complexity of the solution scales as $\mathcal{O}\big(KN(M+1)^2(2M)^{2.5} + (2M)^{3.5}\big)$, or simply as $\mathcal{O}(K^2N^2M^{4.5})$. Furthermore, there are a maximum of $K(M_r+1)M_a$ decision variables in P5** as well as $2M$ constraints. Thus, the complexity of the solution is $\mathcal{O}\big(K(M_r+1){M_a}^2(2M)^{2.5} + (2M)^{3.5}\big)$, or simply $\mathcal{O}\big(K{M_r}^2{M_a}^2M^{4.5}\big)$. Therefore, the overall complexity of the solution to P5 is $\mathcal{O}\big(K^2N^2M^{4.5} + K{M_r}^2{M_a}^2M^{4.5}\big)$. Note that the process of conversion of P5* and P5** into convex problems are of considerably less complexities than the solution to the converted problems and so do not change the mentioned order of overall complexity.

The total computational complexity of the proposed solution to P1, which is represented by Algorithm 3, is calculated by summing the complexity of the subproblems P2, P4, and P5.

IX. Performance evaluation

In this section, we explain the scenario adopted for simulations and we show the performance of our proposed solution and compare it with related existing schemes.

A. Simulation scenario and models

We consider a scenario where the users are distributed both at the proximity of the GBS and fairly away from the GBS. This is a practical scenario as the remote region could represent a disastrous situation to be served via the access FlyBSs that communicate through midway relaying FlyBSs to the GBS. Similar configurations are adopted in many works, e.g., [24], [34], [43], [44], [45].

The simulation area is modeled as rectangular region of a size of $1000m \times 2000m$ with the GBS at one of its corners, as shown in Fig. 5 The region is split by obstacles (e.g. mountains or buildings) to a remote area (size of 1000 m $\times$ 1000 m) and the area in the GBS's proximity (1000 m $\times$ 500 m). Out of all users, 25% and 75% are initially distributed randomly in the GBS's area and over the remote area, respectively. The users move based on a random-walk mobility model with a speed of 1 m/s.

A total bandwidth of 100 MHz is split into 100 channels, each with a bandwidth of 1 MHz. The maximum transmission power of 37 dBm and 30 dBm is considered for the GBS and the FlyBSs, respectively [46]. The noise power is set to -90 dBm [47]. Due to a more dense presence of

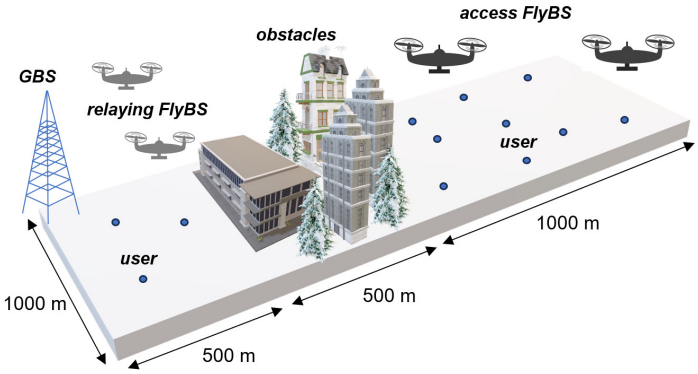

Figure 5: Simulation scenario

obstacles between the two regions (compared to inside of the regions), we consider different pathloss exponents based on the positions of the BSs and the users. In particular, for transmissions between the BS and the user, the pathloss exponent of $\alpha_{n,m} = 2.6$ is assumed. Furthermore, the pathloss exponents of $\alpha_{m,m'} = 2.1$ and $\alpha_{m,m'} = 3.4$ are adopted for the GBS's transmission to the FlyBSs at the relay and at the access link, respectively. Following [40], the channel gain of $g^{SI}_{k,m} = 10^{-6}$ for self-interference is assumed for all channels allocated to the FlyBSs. Omnidirectional antennas with gains 13 dBi, 7 dBi, and 0 dBi are assumed for the GBS, FlyBSs, and users, respectively [46], [48]. An allowed altitude range of $[H_{min,m}, H_{max,m}]$ =[100,300] m and the maximum traveling speed of 20 m/s are assumed for the FlyBSs. The results are shown for $N \in$ [100,300] users and $M \in$ [2,6] FlyBSs with the performance evaluated for different number of FlyBSs at the relay/access link. The results are averaged out over 100 simulation drops, where each simulation is of a duration of 1200 seconds.

We compare our proposal with the following most related recent schemes in the literature: *i*) transmission power allocation, FlyBSs' placement, and association of users for two-hop networks derived from [21] to maximize the sum capacity in a device-to-device network (referred to as *SCDD*) with multiple relaying FlyBSs. Note that, the original work in [21] assumes uplink and downlink users in the device-to-device model. Thus, in order to match their model with ours, we assume that the GBS in our model corresponds to the uplink users. In other words, the uplink users in [21] are all assumed to be located at the GBS's location in our model,
ii) sum rate maximization (referred to as *SRM*) via user association and FlyBSs' positioning in a three-hop network with one relaying FlyBS as introduced in [32].
iii) Maximization of average data rate via positioning and transmission power allocation (referred to as ARPT) in a multiple-FlyBS scenario, as provided in [51].

B. Simulation results

In this subsection, we present and discuss simulation results.

Fig. 6 demonstrates the performance of different schemes in terms of sum capacity for different number of users for a total of $M = 2$ FlyBSs (top figure) and $M = 6$ FlyBSs (bottom figure). Thanks to its flexibility on a setting of the number of

relaying FlyBSs, the performance of the proposal for $M = 6$ is shown for the cases with one and two relaying FlyBSs. Note that, the SRM scheme can adopt only one relaying FlyBS, and an extension of the solution to more relaying FlyBSs is not trivial. The results show that the proposed solution increases the sum capacity compared to SRM, SCDD, and ARPT by 50%, 41%, and 63%, respectively, for $M = 2$, and by 46%, 35%, and 52%, compared to SRM, SCDD, and ARPT, respectively, for $M = 6$.

According to Fig. 6, the sum capacity increases only slightly with the number of users for the proposed scheme. This is due to the fact that the number of users has no significant impact on the interference in the system, as the proposed channel allocation would potentially utilize all available channels regardless of the number of users, and hence, a change of the number of users only causes a rearrangement of assigned channels. The benchmark schemes SRM and SCDD also do not experience any notable change in the sum capacity. This is because both schemes treat the entire available spectrum as a single channel to be used by each FlyBS. Hence, adding more users in the system results in an increase in the channel interference. A similar trend is observed for ARPT. This is because, although the increasing number of users would favorably reduce the average distance between the FlyBS and the users, it would also unfavorably lead to an allocation of smaller bandwidth to each user.

Moreover, regarding the proposed solution, increasing the number of relaying FlyBSs for a fixed M increases the sum capacity only slightly. This is indeed due to a superposition of two opposing effects: i) for a fixed M, having more relaying FlyBSs leads to having fewer access FlyBSs, which limits the sum capacity; ii) having more relaying FlyBSs can potentially provide higher backhaul capacity by providing more channels for backhaul, which gives the FlyBSs a higher freedom of movement due to less restricting constraints on the backhaul (i.e., (13c) and (13d)).

Next, Fig. 7 plots the sum capacity for different number of FlyBSs, different number of relaying FlyBSs, and for $N = 100$ (top figure) and $N = 300$ (bottom figure) for different schemes. Note that the line for each scheme starts from the minimum possible number of FlyBSs. For instance, the proposed solution with two relaying FlyBSs should include at least three FlyBSs considering a minimum of one access FlyBS. According to Fig. 7, the proposed solution increases the sum capacity by 51%, 42%, and 60%, compared to SCDD, SRM, and ARPT, respectively, for N =100. Moreover, for $N = 300$, the proposal increases the sum capacity by 51%, 40%, and 59%, compared to SCDD, SRM, and ARPT, respectively. According to Fig. 7, there is an increasing trend for the sum capacity with the number of FlyBSs (M) for all the schemes. This trend is due to the fact that, the number of users associated to each FlyBS decreases with M and, consequently, decreasing the average distance between the users and the FlyBSs leading to a higher capacity. Furthermore, a larger number of channels can be associated to each FlyBS-user link in general. Moreover, due to an increasing interference in the network (because of channel reuse by different FlyBSs), the sum capacity tends to saturate by increasing M. The sum capacity, however, does not show a tangible trend with the number of relaying FlyBSs for the same M in the proposed solution. This is due to the fact that, despite an increase in the potentially supported capacity over the backhaul link (because of having more relaying FlyBSs), a decrease in the number of access FlyBSs results in an association of more users to each FlyBS resulting in an increase in the average distance between the FlyBSs and the users, and an allocation of a lower number of channels to the FlyBS-user links.

In order to better understand the impact of each of the optimization steps, as illustrated in Fig. 4, we also show the achievable sum capacity in cases when the optimization of one of the variables $\boldsymbol{I}, \boldsymbol{P}, \boldsymbol{A}, \boldsymbol{Q}$ is left out from the proposed solution. Fig. 8 compares the performance of the entire proposed solution with each of such alternatives. According to

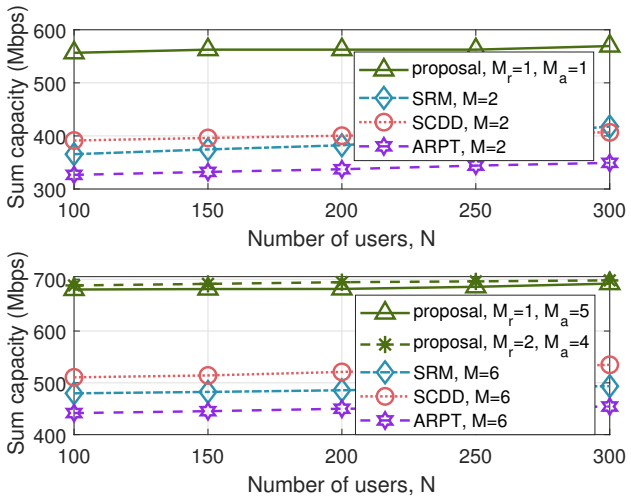

Figure 6: Sum capacity vs. N for different schemes and for different settings of number of relaying FlyBSs (M_r) and number of access FlyBSs (M_a) for $M = 2$ (top plot) and $M = 6$ (bottom plot). The value for M_r in SRM and SCDD is always equal to one and zero, respectively, as assumed by those solutions.

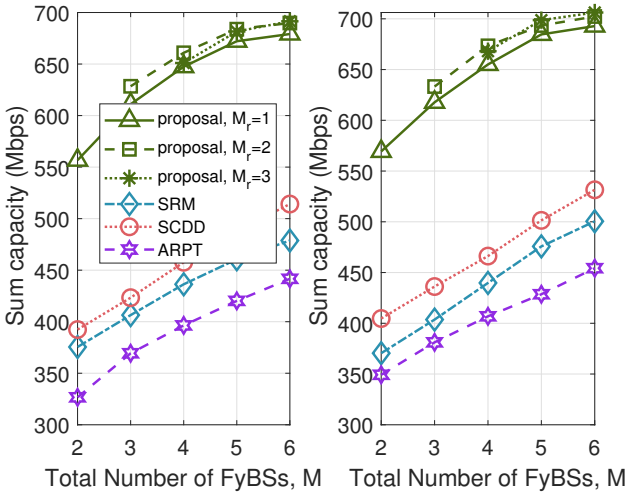

Figure 7: Average user capacity vs. M for different schemes for $N = 100$ (left plot) and $N = 300$ (right plot).

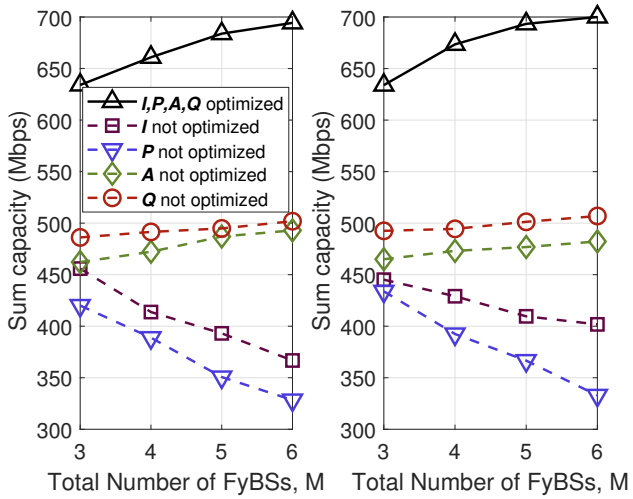

Figure 8: Impact of not optimizing one of the optimization variables throughout the proposed solution for different number of FlyBSs with $M_r = 2$ and for $N = 100$ (left plot) and $N = 300$ (right plot).

Fig. 8, an exclusion of the optimization of $\boldsymbol{I}$, $\boldsymbol{P}$, $\boldsymbol{A}$, and $\boldsymbol{Q}$ degrades the sum capacity with respect to the proposed integrated optimization of all variables by 25%, 33%, 23%, and 19%, respectively, for $N = 100$, and by 20%, 26%, 25%, and 21%, respectively, for $N = 300$. It is observed that the sum capacity decreases with the number of FlyBSs M for the proposed solution if either $\boldsymbol{I}$ or $\boldsymbol{P}$ are not optimized. This is because adding more FlyBSs in the system causes excessive interference, which is not managed via optimization of $\boldsymbol{I}$ or $\boldsymbol{P}$ leading to a degradation in the sum capacity. In case that either $\boldsymbol{A}$ or $\boldsymbol{Q}$ is not optimized, a combination of the optimization of the other three variables still manages to moderate the degradation caused by interference and/or by an increase in the FlyBS-user distances.

Next, Fig. 9 demonstrates fairness among the users (measured as the Jain's fairness index) for different number of users and FlyBSs. The relatively high values of the index (always above 0.8) shown in Fig. 9 indicate that the total provided capacity by the FlyBSs is distributed among the users in a fair way.

Furthermore, we show that the acquired gain in the performance with respect to the existing solutions is not at the cost of excessively energy consuming movements of the FlyBSs. Fig. 10 demonstrates the average incurred propulsion power for different schemes and for different number of FlyBSs, relaying FlyBSs, and users ($N = 100$ and $N = 300$ for the top and bottom subplots, respectively). According to Fig. 10, the energy consumption of the proposal is quite similar to that of SCDD and SRM (less than 5% difference), while the achieved sum capacity is increased up by 51% as shown earlier in this section.

According to Fig. 10, there is an increasing trend in the propulsion power consumption with the number of FlyBSs M for the proposed solution. This is due to the fact that, by increasing M, more interference is introduced in the network. Consequently, a change in the transmission power

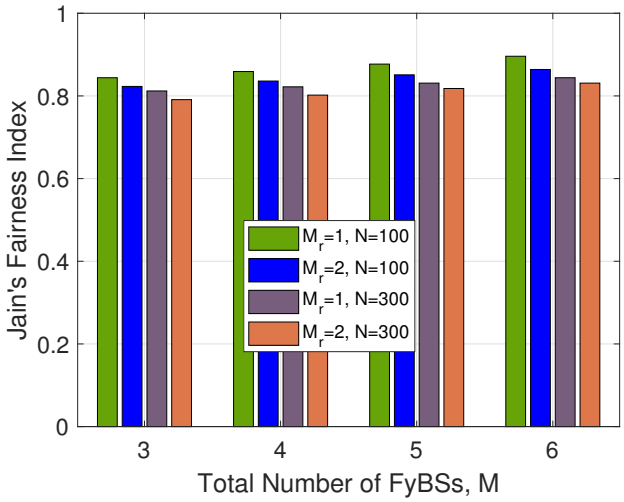

Figure 9: Jain's fairness index among users for different number of users and different number of FlyBSs.

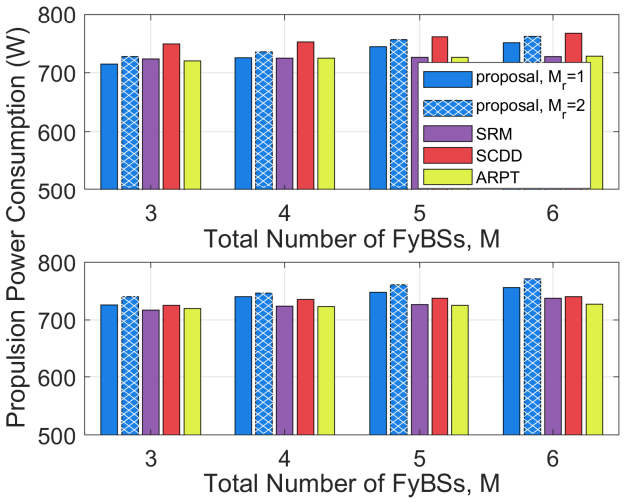

Figure 10: Average propulsion power consumption vs. number of FlyBSs for different schemes.

of the FlyBSs over channels becomes more correlated with the FlyBSs' positioning, necessitating the FlyBSs to relocate more often to alleviate the interference. Furthermore, it is also observed that increasing the number of relaying FlyBSs in the proposed solution increases the propulsion power consumption a bit. This is because, having more relaying FlyBSs gives them more freedom in movement to maximize sum capacity while ensuring the backhaul capacity constraints, which in turn allows more mobility to the access FlyBSs. Moreover, Fig. 10 shows that increasing the number of the users from 100 to 300 results in a decrease in the propulsion power consumption. This is because, by increasing N, a larger number of users are associated with each FlyBS. As a result, the users' movements cancel out each other's effects on the sum capacity by a higher degree, which leads to a less frequent movement of the FlyBSs.

Last, to verify that the iterative manner of the proposed solution does not limit its practical application, we also plot an evolution of the sum capacity in Fig. 11 over iterations of

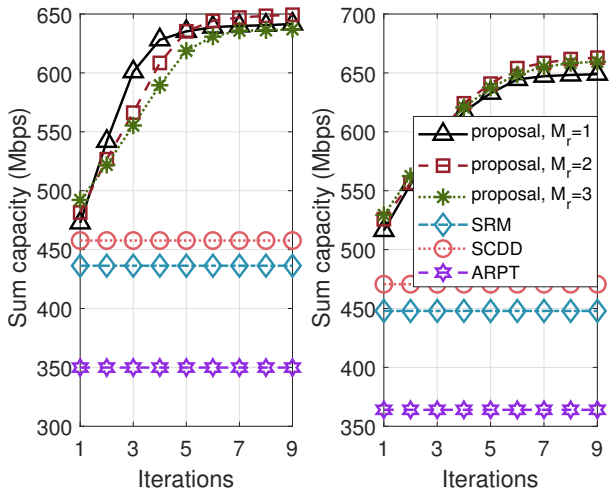

Figure 11: Evolution of sum capacity after each round of the entire proposed optimization for different settings of the number of relaying FlyBSs when $M = 4$ for $N = 100$ (left plot) and $N = 300$ (right plot).

N \ (M_r, M_a)	(1,3)	(1,4)	(1,5)	(2,2)	(2,3)	(2,4)	(3,1)	(3,2)	(3,3)
100	0.28	0.30	0.31	0.29	0.32	0.33	0.29	0.33	0.36
200	0.39	0.44	0.47	0.54	0.57	0.63	0.55	0.60	0.64
300	0.57	0.64	0.68	0.77	0.78	0.81	0.74	0.78	0.83

Table II: Running time (in seconds) of the proposed solution (Algorithm 3) for different numbers of users and FlyBSs

optimization of the variables for different number of relaying FlyBSs and for $N = 100$ (left figure) and $N = 300$ (right figure). Note that, each iteration corresponds to one whole round of optimization as presented in Fig. 4. Four FlyBSs are assumed in both subplots. The lines for SRM, SCDD, and ARPT are only shown for reference. According to Fig. 11, the proposed solution converges quickly and in only few iterations. Furthermore, even after one or two iterations, the proposal outperforms all the schemes SRM, SCDD, and ARPT. Following the fast convergence shown in Fig. 11 in terms of the number of iterations, Table II also indicates the running time (in seconds) of the proposed algorithm, represented by Algorithm 3, using computer with the Intel Core i7-7600U CPU @ 2.80GHz. The duration is shown for different numbers of users and FlyBSs at the relay and access links. According to Table II, the running time is notably shorter than the duration of the selected time steps (i.e., 1 second) in the simulations. This confirms feasibility of the proposed solution even for dense scenarios with high numbers of users and FlyBSs.

X. Conclusions

In this paper, we have studied the problem of sum capacity maximization in multi-hop relaying via FlyBSs. In addition to the direct links between the access FlyBSs and the GBS, a set of relaying FlyBSs are also deployed to improve the communication between the access link and the GBS. The GBS and the relaying FlyBSs can also serve the users directly. Furthermore, to exploit the available radio resources efficiently, a reuse of the channels is allowed at all links. The sum capacity is optimized via an analytical solution based on alternating optimization of FlyBSs' positioning, association of users to FlyBSs, channel allocation, and transmission power allocation. The problem is solved under practical constraints on the FlyBSs' movement as well as on the backhaul capacity. The proposed solution increases the sum capacity by tens of percent compared to the state of the art.

In the future, the problem of resource allocation in multi-hop scenarios with non-orthogonal multiple-access (NOMA) together with related aspects such as clustering, interference cancellation, and decoding shall be studied.

Appendix A
Proof to Proposition 1

Proof. Let us first deal with the non-concavity of the objective with respect to $\boldsymbol{q_m}$ ($m \in \mathcal{M}_A$).

1) Non-concavity of objective in P2:* We derive a concave lower-bound to the objective. To this end, lets rewrite the log(.) term in the capacity in (10) using (7) as

$$\log_2(1+\frac{p^R_{n,m,k}}{\sigma^2_{n,k}+\sum_{m'\in\{a_{n,m'}=0\}} p^R_{n,m',k}}) = \log_2(1+\frac{\kappa_{n,m} d^{-\alpha_{n,m}}_{n,m} p^{TX}_{k,m}}{\sigma^2_{n,k}+\sum_{m'\in\{a_{n,m'}=0\}} \kappa_{n,m',k} d^{-\alpha_{n,m'}}_{n,m'} p^{TX}_{k,m'}}). \tag{30}$$

Next, we provide a lower bound for the interference term in (30), i.e., for $\sum_{m'\in\{a_{n,m'}=0\}} \kappa_{n,m',k} d^{-\alpha_{n,m'}}_{n,m'} p^{TX}_{k,m'}$. We use the fact that the smallest possible distance between the FlyBS m and the user n at the time step t can be derived from their distance at the time step $t-1$ and based on the limitations on the FlyBS's speed. Thus, the distance at the time step t is lower bounded by

$$d_{n,m,min} = ||\boldsymbol{q_m}[t-1] - \boldsymbol{q_n}[t]|| - V_{max}\delta_t, \tag{31}$$

where δ_t is the duration of time step t. Then, using (31), the interference in (30) is upper-bounded as follow

$$\sum_{m'\in\{a_{n,m'}=0\}} \kappa_{n,m',k} d^{-\alpha_{n,m'}}_{n,m'} p^{TX}_{k,m'} \leq \sum_{m'\in\{a_{n,m'}=0\}} \kappa_{n,m',k} d^{-\alpha_{n,m'}}_{n,m',min} p^{TX}_{k,m'}. \tag{32}$$

Next, using the inequality in (32) and by applying $\log_2(1+ax^{-1}) \geq \log_2(1+ax_0^{-1}) - \frac{(x-x_0)}{x_0(a+x_0)\ln(2)}$, we derive an under-estimator for the left-hand-side in (30) as

$$\log_2(1+\frac{\kappa_{n,m}d_{n,m}^{-\alpha_{n,m}}p_{k,m}^{TX}}{\sigma_{n,k}^2+\sum_{m'\in\{a_{n,m'}=0\}}\kappa_{n,m',k}d_{n,m'}^{-\alpha_{n,m'}}p_{k,m'}^{TX}})\geq$$
$$\log_2(1+\frac{\kappa_{n,m,k}d_{n,m}^{-\alpha_{n,m}}p_{k,m}^{TX}}{\sigma_{n,k}^2+\sum_{m'\in\{a_{n,m'}=0\}}\kappa_{n,m',k}d_{n,m',min}^{-\alpha_{n,m'}}p_{k,m'}^{TX}})\geq$$
$$\log_2(1+\eta_{s,n,m}d_{n,m,(0)}^{-\alpha_{n,m}})-\frac{(d_{n,m}^{\alpha_{n,m}}-d_{n,m,(0)}^{\alpha_{n,m}})}{d_{n,m,(0)}^{-\alpha_{n,m}}(\eta_{s,n,m}+d_{n,m,(0)}^{-\alpha_{n,m}})\ln(2)},\tag{33}$$

where the substitution $\eta_{s,n,m}$ is defined as

$$\eta_{s,n,m}=\log_2(1+\frac{\kappa_{n,m,k}p_{k,m}^{TX}}{\sigma_{n,k}^2+\sum_{m'\in\{a_{n,m'}=0\}}\kappa_{n,m',k}d_{n,m',min}^{-\alpha_{n,m'}}p_{k,m'}^{TX}}),\tag{34}$$

and $d_{n,m,(0)}$ is the evaluation of $d_{n,m}$ at the reference point-note that the $d_{n,m,(0)}$ is initially selected arbitrarily whilst fulfilling (13a)-(13f), and then updated by the derived solution from P2*.

The derived lower bound in (33) is concave with respect to the position of access FlyBSs.

2) non-convexity of (13c) in P2:* Next, we address the non-convexity in (13c). In particular, we first derive a lower bound for the term $\sum_{m'\in\mathcal{M}_{\mathcal{R}}}C_{m,m'}$ in (13c), and an upper bound for the term $\sum_{n=1}^{N}a_{n,m}C_{n,m}$ in (13c), such that the resulting derived (tighter) constraint would define a convex space for $\boldsymbol{Q}$. To this end, using (8), the log(.) term in $C_{m,m'}$ (as shown in (11)) is first rewritten to

$$\log_2(1+\frac{p_{m,m',k}^{R}}{\sigma_{m,k}^2+g_{k,m}^{SI}p_{k,m}^{TX}+\sum\limits_{m''\in\mathcal{M}_{\mathcal{R}}\cup\{0\}-\{m'\}}p_{m,m'',k}^{R}})=\log_2(1+$$
$$\frac{\kappa_{m,m',k}d_{m,m'}^{-\alpha_{m,m'}}p_{k,m'}^{TX}}{\sigma_{m,k}^2+g_{k,m}^{SI}p_{k,m}^{TX}+\sum\limits_{m''\in\mathcal{M}_{\mathcal{R}}\cup\{0\}-\{m'\}}\kappa_{m,m'',k}d_{m,m''}^{-\alpha_{m,m''}}p_{k,m''}^{TX}}).\tag{35}$$

Furthermore, we find an upper bound for the interference term in (35). To do so, we determine the maximum possible distance $d_{m,m',min}$ between the FlyBSs m and m' at the time step t using their distance at the time step $t-1$ and the maximum speed of the FlyBSs, i.e.,

$$d_{m,m',min}=||\boldsymbol{q_m}[t-1]-\boldsymbol{q_{m'}}[t-1]||-2V_{max}\delta_t.\tag{36}$$

Then, the lower bound for $\sum_{m'\in\mathcal{M}_{\mathcal{R}}}C_{m,m'}$ can be derived similarly as in (33), which yields a concave expression with respect to $\boldsymbol{Q}$.

Next, we derive an upper bound for $\sum_{n=1}^{N}a_{n,m}C_{n,m}$. To this end, we use the fact that the maximum distance between the FlyBS m and the user n at the time t can be determined from their distance at the previous time step $t-1$ and from the maximum possible displacement of the FlyBS. The maximum possible distance $d_{n,m,max}[t]$ between the FlyBS m and the user n is

$$d_{n,m,max}=||\boldsymbol{q_m}[t-1]-\boldsymbol{q_n}[t]||+V_{max}\delta_t.\tag{37}$$

From (30), (31), and (37) the log(.) term in the sum capacity is upper bounded as

$$\log_2(1+\frac{\kappa_{n,m,k}d_{n,m}^{-\alpha_{n,m}}p_{k,m}^{TX}}{\sigma_{n,k}^2+\sum_{m'\in\{a_{n,m'}=0\}}\kappa_{n,m',k}d_{n,m'}^{-\alpha_{n,m'}}p_{k,m'}^{TX}})\leq$$
$$\log_2(1+\frac{\kappa_{n,m,k}d_{n,m,min}^{-\alpha_{n,m}}p_{k,m}^{TX}}{\sigma_{n,k}^2+\sum_{m'\in\{a_{n,m'}=0\}}\kappa_{n,m',k}d_{n,m',max}^{-\alpha_{n,m'}}p_{k,m'}^{TX}}).\tag{38}$$

Hence, (13c) is replaced by the a substitute constraint so that the left-hand side of (13c) adopts the upper bound in (38) instead of the log(.) term, and the right-hand side adopts the lower bound in (33) instead of the log(.) term. The resulting substitute constraint is then convex with respect to $\boldsymbol{Q}$.

3) non-convexity of (13d) in P2:* As the last step to cure P2*, we now deal with the constraint (13d). Note that the term $C_{n,m'}$, $C_{m',m}$, and $C_{0,m'}$ are all non-convex with respect to $\boldsymbol{q_m}$ ($m\in\mathcal{M}_{\mathcal{A}}$). Similar to the procedure for (13c), we derive an alternative constraint to (13d) such that, upon fulfillment of the alternative, the original constraint (13d) would be fulfilled as well. To this end, a convex/concave upper/lower bound for the left-/right-hand side in(13d) is derived as follow. For the term $C_{n,m'}$, a similar approach to the derivation of (38) (for $C_{n,m}$) is taken. Next, for $C_{m',m}$, the log(.) term (as in (11)) is rewritten and then upper-bounded as follow

$$\log_2(1+\frac{p_{m,m',k}^{R}}{\sigma_{m,k}^2+g_{k,m}^{SI}p_{k,m}^{TX}+\sum\limits_{m''\in\mathcal{M}_{\mathcal{R}}\cup\{0\}-\{m'\}}p_{m,m'',k}^{R}})=\log_2(1$$
$$+\frac{\kappa_{m,m',k}p_{k,m'}^{TX}d_{m,m'}^{-\alpha_{m,m'}}}{\zeta_{m,m',k}})\leq\log_2(1+\frac{\kappa_{m,m',k}p_{k,m'}^{TX}}{\zeta_{m,m',k,min}d_{m,m'}^{\alpha_{m,m'}}})=\log_2($$
$$\kappa_{m,m',k}p_{k,m'}^{TX}+\zeta_{m,m',k,min}d_{m,m'}^{\alpha_{m,m'}})-\zeta_{m,m',k,min}\log_2(d_{m,m'}^{\alpha_{m,m'}})=$$
$$\zeta_{m,m',k,min}\log_2(\frac{\kappa_{m,m',k}p_{k,m'}^{TX}}{\zeta_{m,m',k,min}}+d_{m,m'}^{\alpha_{m,m'}})-$$
$$\zeta_{m,m',k,min}\log_2(d_{m,m'}^{\alpha_{m,m'}})\leq\zeta_{m,m',k,min}\big(\log_2(\frac{\kappa_{m,m',k}p_{k,m'}^{TX}}{\zeta_{m,m',k,min}}+$$
$$d_{m,m',(0)}^{\alpha_{m,m'}})+\Delta_{m,m',k}(d_{m,m'}^{\alpha_{m,m'}}-d_{m,m',(0)}^{\alpha_{m,m'}})\big)-$$
$$\zeta_{m,m',k,min}\log_2(d_{m,m',min}^{\alpha_{m,m'}}),\tag{39}$$

where

$$\zeta_{m,m',k}=\sigma_{m,k}^2+g_{k,m}^{SI}p_{k,m}^{TX}+\sum_{m''\in\mathcal{M}_{\mathcal{R}}\cup\{0\}-\{m'\}}\kappa_{m,m'',k}d_{m,m''}^{-\alpha_{m,m''}}p_{k,m''}^{TX},$$
$$\zeta_{m,m',k,min}=\sigma_{m,k}^2+g_{k,m}^{SI}p_{k,m}^{TX}+\sum_{m''\in\mathcal{M}_{\mathcal{R}}\cup\{0\}-\{m'\}}\kappa_{m,m'',k}d_{m,m'',max}^{-\alpha_{m,m''}}p_{k,m''}^{TX},$$
$$\Delta_{m,m',k}=\frac{1}{(\frac{\kappa_{m,m',k}p_{k,m'}^{TX}}{\zeta_{m,m',k,min}}+d_{m,m',(0)}^{\alpha_{m,m'}})\ln(2)},\tag{40}$$

and $d_{m,m',max}$ in (40) is the maximum distance between the FlyBSs m and m'' that can occur at the time step t. The maximum distance is determined from the distance between the FlyBSs at the time step $t-1$ as well as from to the FlyBSs' maximum speed as

$$d_{m,m'',max}=||\boldsymbol{q_m}[t-1]-\boldsymbol{q_{m''}}[t-1]||+2V_{max}\delta_t.\tag{41}$$

Note that the derived upper bound in 39) is convex with respect to $\boldsymbol{q_m}$ ($m\in[1,M_a]$).

As the final step in treating the constraint (13d) for the formulated problem P2*, we derive a concave lower bound for $C_{0,m'}$. To this end, the log(.) term in $C_{0,m'}$ is first rewritten and lower bounded as

$$\log_2(1+\frac{p^R_{m',0,k}}{\sigma^2_{m',k}+g^{SI}_{k,m'}p^{TX}_{k,m'}+\sum\limits_{m''\in\mathcal{M}_{\mathcal{A}}}p^R_{m,m'',k}})=\log_2(1+\frac{\kappa_{m',0,k}d^{-\alpha_{m',0}}_{m',0}p^{TX}_{k,0}}{\sigma^2_{m',k}+g^{SI}_{k,m'}p^{TX}_{k,m'}+\sum\limits_{m''\in\mathcal{M}_{\mathcal{A}}}\kappa_{m',m'',k}d^{-\alpha_{m',m''}}_{m',m''}p^{TX}_{k,m''}})\geq \log_2(1+\frac{\kappa_{m',0,k}d^{-\alpha_{m',0}}_{m',0}p^{TX}_{k,0}}{\sigma^2_{m',k}+g^{SI}_{k,m'}p^{TX}_{k,m'}+\sum\limits_{m''\in\mathcal{M}_{\mathcal{A}}}\kappa_{m',m'',k}d^{-\alpha_{m',m''}}_{m',m'',min}p^{TX}_{k,m''}}). \tag{42}$$

Then, the right-hand-side in (42) is lower bounded using the inequality $\log_2(1+ax^{-1})\geq\log_2(1+ax_0^{-1})-\frac{(x-x_0)}{x_0(a+x_0)\ln(2)}$ with the variable x representing $d^{\alpha_{m',0}}_{m',0}$. The procedure follows the derivation in (33). Details are omitted due to space limitation. □

Appendix B
Proof to Proposition 2

*1) Non-concavity of objective in P2**:* In order to derive a concave objective from the sum capacity, we find a lower bound to the log(.) term in the sum capacity as follows

$$\log_2(1+\frac{\kappa_{n,m,k}d^{-\alpha_{n,m}}_{n,m}p^{TX}_{k,m}}{\sigma^2_{n,k}+\sum_{m'\in\{a_{n,m'}=0\}}\kappa_{n,m',k}d^{-\alpha_{n,m'}}_{n,m'}p^{TX}_{k,m'}})=\log_2(\sigma^2_{n,k}+\sum_m\kappa_{n,m,k}d^{-\alpha_{n,m}}_{n,m}p^{TX}_{k,m})-\log_2(\sigma^2_{n,k}+\sum_{m'\in\{a_{n,m'}=0\}}\kappa_{n,m',k}d^{-\alpha_{n,m'}}_{n,m'}p^{TX}_{k,m'})\geq\log_2(\sigma^2_{n,k}+\sum_m\kappa_{n,m,k}d^{-\alpha_{n,m}}_{n,m}p^{TX}_{k,m})-\log_2(\sigma^2_{n,k}+\sum_{m'\in\{a_{n,m'}=0\}}\kappa_{n,m',k}d^{-\alpha_{n,m'}}_{n,m',min}p^{TX}_{k,m'})=\frac{1}{M_r}\big(\sum_{m'}\log_2(\Phi_{n,m,m'}+\kappa_{n,m',k}d^{-\alpha_{n,m'}}_{n,m'}p^{TX}_{k,m'})\big)-\log_2(\sigma^2_{n,k}+\sum_{m'\in\{a_{n,m'}=0\}}\kappa_{n,m',k}\times d^{-\alpha_{n,m'}}_{n,m',min}p^{TX}_{k,m'})\geq\frac{1}{M_r}\Big(\sum_{m'}\big(\log_2(\Phi_{n,m,m',min}+\kappa_{n,m',k}d^{-\alpha_{n,m'}}_{n,m',(0)}p^{TX}_{k,m'})-\Xi_{n,m,m',k}(d^{\alpha_{n,m'}}_{n,m'}-d^{\alpha_{n,m'}}_{n,m',(0)})\big)\Big)-\log_2(\sigma^2_{n,k}+\sum_{m'\in\{a_{n,m'}=0\}}\kappa_{n,m',k}d^{-\alpha_{n,m'}}_{n,m',min}p^{TX}_{k,m'}), \tag{43}$$

where

$$\Phi_{n,m,m'}=\sigma^2_{n,k}+\sum_{m\in\mathcal{M}-\{m'\}}\kappa_{n,m',k}d^{-\alpha_{n,m'}}_{n,m'}p^{TX}_{k,m'} \tag{44}$$

$$\Phi_{n,m,m',min}=\sigma^2_{n,k}+\sum_{m\in\mathcal{M}-\{m'\}}\kappa_{n,m',k}d^{-\alpha_{n,m'}}_{n,m',max}p^{TX}_{k,m'},$$

$$\Xi_{n,m,m',k}=d^{\alpha_{n,m'}}_{n,m',(0)}(\frac{\kappa_{n,m',k}p^{TX}_{k,m'}}{\Phi_{n,m,m',min}}+d^{\alpha_{n,m'}}_{n,m',(0)})\ln(2),$$

and $d_{n,m',(0)}$ is the evaluation of $d_{n,m'}$ at the reference point (0). Note that the brackets in $d_{n,m',(0)}$ are used so as not to confuse the reference points with the index 0 used for the GBS. The value of $d_{n,m,(0)}$ in practice is initially selected arbitrarily to fulfill (13a)-(13f), and then updated by the derived solution from P2**. Also note that, the value of $d_{n,m',(0)}$ for the access FlyBSs are the same as their actual value, since those FlyBSs are at fixed points when targeting the placement of the relays. The derived lower bound in (43) is now concave with respect to $\boldsymbol{q_{m'}}$ ($m'\in\mathcal{M}_{\mathcal{R}}$).

*2) Non-convexity of (13c) in P2**:* Next, a convex constraint is derived from (13c) via replacing the left-hand and right-hand sides in (13c) by convex upper bound and concave lower bounds, respectively. To this end, for the left-hand side in (13c), the log(.) term in the capacity is first rewritten and then upper bounded as

$$\log_2(1+\frac{\kappa_{n,m,k}d^{-\alpha_{n,m}}_{n,m}p^{TX}_{k,m}}{\sigma^2_{n,k}+\sum_{m'\in\{a_{n,m'}=0\}}\kappa_{n,m',k}d^{-\alpha_{n,m'}}_{n,m'}p^{TX}_{k,m'}})=\log_2(\sigma^2_{n,k}+\sum_m\kappa_{n,m,k}d^{-\alpha_{n,m}}_{n,m}p^{TX}_{k,m})-\log_2(\sigma^2_{n,k}+\sum_{m'\in\{a_{n,m'}=0\}}\kappa_{n,m',k}\times d^{-\alpha_{n,m'}}_{n,m'}p^{TX}_{k,m'})\leq\log_2(\sigma^2_{n,k}+\sum_m\kappa_{n,m,k}d^{-\alpha_{n,m}}_{n,m,min}p^{TX}_{k,m})-\log_2(\sigma^2_{n,k}+\sum_{m'\in\{a_{n,m'}=0\}}\kappa_{n,m',k}d^{-\alpha_{n,m'}}_{n,m'}p^{TX}_{k,m'}). \tag{45}$$

Then, a lower bound to the subtrahend right-hand side in (45) is derived by applying a similar approach as to (43). The resulting upper bound (not shown here to save space) is then convex.

Next, a derivation of convex lower bound to $\sum_{m'\in\mathcal{M}_{\mathcal{R}}}C_{m,m'}$ is provided similarly as in the proposed process for positioning of the access FlyBSs (see (35) and the discussion after). With the proposed replacements above, (13c) is converted into a convex constraint.

*3) Non-convexity of (13d) in P2**:* Next, to tackle non-convexity with (13d), let us note that the term $C_{n,m'}$ in (13d) is upper bounded via a process similar to the derivation of convex upper bound to $C_{n,m}$ as explained above (see (45)).

Next, to deal with the non-convexity of $C_{m',m}$, the log(.) term (as in (11)) is rewritten using (40), and then upper-bounded as follow

$$\log_2(1+\frac{p^R_{m,m',k}}{\sigma^2_{m,k}+g^{SI}_{k,m}p^{TX}_{k,m}+\sum\limits_{m''\in\mathcal{M}_{\mathcal{R}}\cup\{0\}-\{m'\}}p^R_{m,m'',k}})=\log_2(\zeta_{m,m'}+\kappa_{m,m',k}d^{-\alpha_{m,m'}}_{m,m'}p^{TX}_{k,m'})-\log_2(\sigma^2_{m,k}+g^{SI}_{k,m}p^{TX}_{k,m}+\sum_{m''\in\mathcal{M}_{\mathcal{R}}\cup\{0\}-\{m'\}}\kappa_{m,m'',k}d^{-\alpha_{m,m''}}_{m,m''}p^{TX}_{k,m''})\leq\log_2(\zeta_{m,m',max}+\kappa_{m,m',k}d^{-\alpha_{m,m'}}_{m,m',min}p^{TX}_{k,m'})-\log_2(\sigma^2_{m,k}+g^{SI}_{k,m}p^{TX}_{k,m}+\sum_{m''\in\mathcal{M}_{\mathcal{R}}\cup\{0\}-\{m'\}}\kappa_{m,m'',k}d^{-\alpha_{m,m''}}_{m,m''}p^{TX}_{k,m''}), \tag{46}$$

where

$$\zeta_{max} = \sigma^2_{m,k} + g^{SI}_{k,m} p^{TX}_{k,m} + \sum_{m'' \in \mathcal{M}_{\mathcal{R}} \cup \{0\} - \{m'\}} \kappa_{m,m'',k} d^{-\alpha_{m,m''}}_{m,m'',min} p^{TX}_{k,m''}. \quad (47)$$

Then, the subtrahend log(.) term on the right-hand side in (46) is upper bounded by a convex function via a similar approach as applied for the upper bound of the log(.) term in (45).

Last, we deal with the non-concavity of $C_{0,m'}$ in (13d). We derive a concave lower bound to the log(.) term in $C_{0,m'}$ (according to (12)) as follows

$$\log_2(1 + \frac{p^R_{m',0,k}}{\sigma^2_{m',k} + g^{SI}_{k,m'} p^{TX}_{k,m'} + \sum_{m'' \in \mathcal{M}_{\mathcal{A}}} p^R_{m,m'',k}}) =$$

$$\log_2(1 + \frac{\kappa_{m',0,k} d^{-\alpha_{m',0}}_{m',0} p^{TX}_{k,0}}{\sigma^2_{m',k} + g^{SI}_{k,m'} p^{TX}_{k,m'} + \sum_{m'' \in \mathcal{M}_{\mathcal{A}}} \kappa_{m',m'',k} d^{-\alpha_{m',m''}}_{m',m''} p^{TX}_{k,m''}}) =$$

$$\log_2(\sigma^2_{m',k} + g^{SI}_{k,m'} p^{TX}_{k,m'} + \sum_{m'' \in \mathcal{M}_{\mathcal{A}}} \kappa_{m',m'',k} d^{-\alpha_{m',m''}}_{m',m''} p^{TX}_{k,m''} + \kappa_{m',0,k} d^{-\alpha_{m',0}}_{m',0} p^{TX}_{k,0}) - \log_2(\sigma^2_{m',k} + g^{SI}_{k,m'} p^{TX}_{k,m'} +$$

$$\sum_{m'' \in \mathcal{M}_{\mathcal{A}}} \kappa_{m',m'',k} d^{-\alpha_{m',m''}}_{m',m''} p^{TX}_{k,m''}) \geq \log_2(\sigma^2_{m',k} + g^{SI}_{k,m'} p^{TX}_{k,m'} + \sum_{m'' \in \mathcal{M}_{\mathcal{A}}} \kappa_{m',m'',k} d^{-\alpha_{m',m''}}_{m',m''} p^{TX}_{k,m''} + \kappa_{m',0,k} d^{-\alpha_{m',0}}_{m',0} p^{TX}_{k,0}) -$$

$$\varrho_{m,m',k,min} = \frac{1}{M_a + 1} \sum_{m \in \mathcal{M}_{\mathcal{A}}} \log_2(\Theta_{m,m'} + \kappa_{m',m'',k} d^{-\alpha_{m',m''}}_{m',m''} p^{TX}_{k,0})$$

$$-\varrho_{m,m',k,min} \geq \frac{1}{M_a + 1} \sum_{m} \log_2(\Theta_{m,m',min} + \kappa_{m,m',k} d^{-\alpha_{m,m'}}_{m,m'} \times p^{TX}_{k,0}) - \varrho_{m,m',k,min} \geq \frac{1}{M_a + 1} \Big(\sum_{m'} \log_2(\Theta_{m,m',min} + \kappa_{m,m',k} \times d^{-\alpha_{m,m'}}_{m,m',(0)} p^{TX}_{k,m'}) - \epsilon_{m,m',k} (d^{\alpha_{m,m'}}_{m,m'} - d^{\alpha_{m,m'}}_{m,m',(0)}) \Big) - \varrho_{m,m',k,min}, \quad (48)$$

where

$$\Theta_{m,m'} = \sigma^2_{m',k} + g^{SI}_{k,m'} p^{TX}_{k,m'} + \sum_{m'' \in \mathcal{M}_{\mathcal{A}} \cup \{0\} - \{m\}} \kappa_{m',m'',k} d^{-\alpha_{m',m''}}_{m',m''} p^{TX}_{k,m''},$$

$$\Theta_{m,m',min} = \sigma^2_{m',k} + g^{SI}_{k,m'} p^{TX}_{k,m'} + \sum_{m'' \in \mathcal{M}_{\mathcal{A}} \cup \{0\} - \{m\}} \kappa_{m',m'',k} d^{-\alpha_{m',m''}}_{m',m'',max} p^{TX}_{k,m''},$$

$$\varrho_{m,m',k,min} = \log_2(\sigma^2_{m',k} + g^{SI}_{k,m'} p^{TX}_{k,m'} + \sum_{m'' \in \mathcal{M}_{\mathcal{A}}} \kappa_{m',m'',k} d^{-\alpha_{m',m''}}_{m',m'',min} p^{TX}_{k,m''}),$$

$$\epsilon_{m,m',k} = \frac{1}{d^{\alpha_{m,m'}}_{m,m',(0)} (\frac{\kappa_{m,m',k} p^{TX}_{k,m'}}{\Phi_{m,m',min}} + d^{\alpha_{m,m'}}_{m,m',(0)}) \ln(2)}. \quad (49)$$

The resulting lower bound in (49) is concave with respect to the relaying FlyBSs' positions $\boldsymbol{q_{m'}}$ ($m' \in \mathcal{M}_{\mathcal{R}}$).

Appendix C
Proposition 3: Determination of ι_{max}

Without a consideration of the backhaul constraints (13c) and (13d), it is evident that having a higher BS-user overall capacity does not guarantee a higher total capacity in the network. This is because the actual overall capacity that each BS could provide is still limited by the overall capacity of the backhaul links connected to that BS. In the light of this fact, it is not suitable to relax the backhaul constraints in P5 without adding any backup constraint, since it could lead to solutions with an excessive amount of channels allocated to the BS-user links resulting in insufficient capacities over the backhaul. To tackle this issue, the parameter ι_{max} is introduced to limit the maximum number of channels that can be assigned to each BS-user link.

An analytical determination of ι_{max}, however, is quite difficult if not impossible, as the subsequent optimization of transmission power could have a large impact on the capacities of the BS-BS and user-BS links, and hence on ι_{max}. Thus, a realistic approach is to regulate ι_{max} according to the actual values of the link capacities. More specifically, the value of ι_{max} is determined for each iteration of the alternating optimization of $\{\boldsymbol{I}, \boldsymbol{P}, \boldsymbol{A}, \boldsymbol{Q}\}$ as explained in the following. First, ι_{max} is initialized by the total number of channels, i.e., K. Then, one round of optimization of $\{\boldsymbol{I}, \boldsymbol{P}, \boldsymbol{A}, \boldsymbol{Q}\}$ is performed with $\boldsymbol{I}$ and $\boldsymbol{A}$ determined via solving P4 and with respect to the adopted ι_{max}. Then, the total network's capacity is calculated at the derived values of $\{\boldsymbol{I}, \boldsymbol{P}, \boldsymbol{A}, \boldsymbol{Q}\}$. Next, the same procedure is repeated for $\iota_{max} = K - 1$, and so on. It is expected that at some point for some value of ι_{max}, say $\iota_{max} = \iota^*_{max}$, the total capacity of network reaches its maximum, and then starts to decrease for $\iota_{max} > \iota^*_{max}$. Then the optimal value of ι_{max} for the considered iteration is set to be ι^*_{max}. The optimal value of ι_{max} is determined for next iterations likewise.

Appendix D
Proof to Proposition 4

To solve the problem in P5*, since the objective is non-concave with respect to $p^{TX}_{k,m}$, we first substitute the objective with a concave under-estimator. To this end, the log(.) term in (10) is expanded and, then, lower bounded by applying the inequality $\log_2(a+x) \leq \log_2(a+x_0) + \frac{(x-x_0)}{(a+x_0)\ln(2)}$ as follows (the time index "$[t]$" is omitted to avoid cluttering)

$$\log_2(1 + \frac{p^R_{n,m,k}}{\sigma^2_{n,k} + \sum_{m' \in \{a_{n,m'}=0\}} p^R_{n,m',k}}) = \log_2(\sigma^2_{n,k} + \sum_{m \in \mathcal{M}} p^R_{n,m,k}) - \log_2(\sigma^2_{n,k} + \sum_{m' \in \{a_{n,m'}=0\}} p^R_{n,m',k}) \geq$$

$$\log_2(\sigma^2_{n,k} + \sum_{m \in \mathcal{M}} p^R_{n,m,k}) - \big(\log_2(\sigma^2_{n,k} + \sum_{m' \in \{a_{n,m'}=0\}} p^R_{n,m',k,(0)}) + \frac{\sum_{m' \in \{a_{n,m'}=0\}} p^R_{n,m',k} - \sum_{m' \in \{a_{n,m'}=0\}} p^R_{n,m',k,(0)}}{(\sigma^2_{n,k} + \sum_{m' \in \{a_{n,m'}=0\}} p^R_{n,m',k,(0)}) \ln(2)}\big). \quad (50)$$

where $p^R_{n,m',k,(0)}$ is the evaluation of $p^R_{n,m',k}$ at the reference point for $p^{TX}_{k,m',(0)}$ and according to (8). Initially, the value of $p^R_{n,m',k,(0)}$ is selected arbitrarily provided that the constraints (13c), (13d), (13e) are fulfilled. Note that the value of $p^R_{n,m',k}$

derived from the solution to P5* is selected as the reference value of $p^R_{n,m',k,(0)}$ for the next iteration.

The derived lower bound in (50) is concave with respect to $p^R_{n,m',k}$ and, hence, with respect to $p^{TX}_{k,m}$ according to (7). Subsequently, a concave expression can be derived for sum capacity.

Next, the constraint (13c) is first rewritten as

$$\sum_{n=1}^{N}\sum_{k'\in\boldsymbol{k_n}} a_{n,m}B_{k'}\log_2(1+\frac{p^R_{n,m,k}}{\sigma^2_{n,k}+\sum_{m'\in\{a_{n,m'}=0\}}p^R_{n,m',k'}}) \leq \sum_{m'\in\mathcal{M}_{\mathcal{R}}}\sum_{k\in I_{m,m'}} B_k\log_2(1+ \frac{p^R_{m,m',k}}{\sigma^2_{m,k}+g^{SI}_{k,m}p^{TX}_{k,m}+\sum_{m''\in\mathcal{M}_{\mathcal{R}}\cup\{0\}-\{m'\}}p^R_{m,m'',k}}), \quad (51)$$

Then, using the inequality $\log_2(1+\frac{a}{b+kx}) \geq \log_2(1+\frac{a}{b+kx_0}) - \frac{k(x-x_0)}{(b+kx_0)(a+b+kx_0)\ln(2)}$ for $a,k>0$ and arbitrary $x_0 > \frac{-b}{k}$, we derive an under-estimator for the log(.) term on the right-hand-side in (51) (with $p^{TX}_{k,m}$ being the corresponding x in the mentioned inequality) as follows

$$\log_2(1+\frac{p^R_{m,m',k}}{\sigma^2_{m,k}+\sum_{m''\in\mathcal{M}_{\mathcal{R}}\cup\{0\}-\{m'\}}p^R_{m,m'',k}+g^{SI}_{k,m}p^{TX}_{k,m}}) =$$

$$\log_2(1+\frac{p^R_{m,m',k}}{\Gamma_{m,m',k}+g^{SI}_{k,m}p^{TX}_{k,m}}) \geq \log_2(1+\frac{p^R_{m,m',k}}{\Gamma_{m,m',k}+g^{SI}_{k,m}p^{TX}_{k,m,(0)}}) - \varepsilon_{m,m',k}(p^{TX}_{k,m}-p^{TX}_{k,m,(0)}), \quad (52)$$

where

$$\Gamma_{m,m',k} = \sigma^2_{m,k}+\sum_{m''\in\mathcal{M}_{\mathcal{R}}\cup\{0\}-\{m'\}}p^R_{m,m'',k},$$

$$\varepsilon_{m,m',k} = \frac{g^{SI}_{k,m}}{(\Gamma_{m,m',k}+g^{SI}_{k,m}p^{TX}_{k,m,(0)})(p^R_{m,m',k}+\Gamma_{m,m',k}+g^{SI}_{k,m}p^{TX}_{k,m,(0)})\ln(2)}. \quad (53)$$

The right-hand side in (52) is linear with respect to $p^{TX}_{k,m}$. Next, as for the left-hand side in (51), the log(.) term on is first expanded as

$$\log_2(1+\frac{p^R_{n,m,k}}{\sigma^2_{n,k}+\sum_{m'\in\{a_{n,m'}=0\}}p^R_{n,m',k}}) = \log_2(\sigma^2_{n,k}+\sum_{m'\in\{a_{n,m'}=0\}}\kappa_{n,m',k}d^{-\alpha_{n,m'}}_{n,m'}p^{TX}_{k,m'}+\kappa_{n,m,k}d^{-\alpha_{n,m}}_{n,m}p^{TX}_{k,m}) - \log_2(\sigma^2_{n,k}+\sum_{m'\in\{a_{n,m'}=0\}}p^R_{n,m',k}) =$$

$$\log_2(\sigma^2_{n,k}+\sum_{m\in\mathcal{M}}\kappa_{n,m,k}d^{-\alpha_{n,m}}_{n,m}p^{TX}_{k,m}) - \log_2(\sigma^2_{n,k}+\sum_{m'\in\{a_{n,m'}=0\}}\kappa_{n,m',k}d^{-\alpha_{n,m'}}_{n,m'}p^{TX}_{k,m'}). \quad (54)$$

Then, by applying the inequality $\log_2(a+x) \leq \log_2(a+x_0)+\frac{(x-x_0)}{(a+x_0)\ln(2)}$ (for $k>0$ and arbitrary x) to derive an over-estimator to the second term on the right-hand side in (54), we get

$$\log_2(1+\frac{p^R_{n,m,k}}{\sigma^2_{n,k}+\sum_{m'\in\{a_{n,m'}=0\}}p^R_{n,m',k}}) \leq \log_2(\sigma^2_{n,k}+\sum_{m\in\mathcal{M}}\kappa_{n,m,k}d^{-\alpha_{n,m}}_{n,m}p^{TX}_{k,m}) - \Big(\log_2(\sigma^2_{n,k}+\sum_{m'\in\{a_{n,m'}=0\}}p^R_{n,m',k,(0)}) + \frac{\sum_{m'\in\{a_{n,m'}=0\}}\kappa_{n,m',k}d^{-\alpha_{n,m'}}_{n,m'}p^{TX}_{k,m'} - \sum_{m'\in\{a_{n,m'}=0\}}p^R_{n,m',k,(0)}}{(\sigma^2_{n,k}+\sum_{m'\in\{a_{n,m'}=0\}}p^R_{n,m',k,(0)})\ln(2)}\Big). \quad (55)$$

The derived upper bound in (55) is now convex with respect to the transmission power over the access links (i.e., $p^{TX}_{k,m}$ and $p^{TX}_{k,m'}$ in (55)).

Next, the first term on the left-hand side in (13d) is neither convex nor concave with respect to the transmission power over the access links (the second terms is convex). Furthermore, the right-hand side in (13d) is convex. Hence, we propose to replace (13d) with a convex constraint such that, by fulfilling the substitute constraint, (13d) would be automatically fulfilled as well. More specifically, we derive a convex upper bound for the left-hand side in (13d), and a concave lower bound for the right-hand side in (13d). To this end, for the term $\sum_{n=1}^{N}a_{n,m'}C_{n,m'}$, we take a similar procedure as in the derivation of (55) for $\sum_{n=1}^{N}a_{n,m}C_{n,m}$ to get a convex upper bound (the derivation is not included to avoid cluttering). Furthermore, for the term $C_{0,m'}$ in (13d), we adopt a similar derivation as in (52) (which is for $C_{m,m'}$). Therefore, the problem P5* is replaced by the problem of maximization of a concave objective under convex constraints, which is solved using CVX.

Appendix E
Proof to Proposition 5

To solve the problem in P5**, it is observed from (10) that the objective is convex with respect to the transmission power over the BS-BS link. Nevertheless, the constraint (13c) is non-convex with respect to $p^{TX}_{k,m'}$. To tackle the non-convexity, we derive a lower bound for the right-hand side in (13c) to be concave with respect to $p^{TX}_{k,m'}$. More specifically, using the inequality $\log_2(a+x) \leq \log_2(a+x_0)+\frac{(x-x_0)}{(a+x_0)\ln(2)}$, the log(.) term in the right-hand side in (13c) is rewritten and then lower bounded as

$$\log_2(1+\frac{p^R_{m,m',k}}{\sigma^2_{m,k}+g^{SI}_{k,m}p^{TX}_{k,m}+\sum_{m''\in\mathcal{M}_{\mathcal{R}}\cup\{0\}-\{m'\}}p^R_{m,m'',k}}) = \log_2(\Psi_{k,m}+\sum_{m''\in\mathcal{M}_{\mathcal{R}}\cup\{0\}}p^R_{m,m'',k}) - \log_2(\Psi_{k,m}+\sum_{m''\in\mathcal{M}_{\mathcal{R}}\cup\{0\}-\{m'\}}p^R_{m,m'',k}) \geq \log_2(\Psi_{k,m}+\sum_{m''\in\mathcal{M}_{\mathcal{R}}\cup\{0\}}p^R_{m,m'',k}) - \Big(\log_2(\Psi_{k,m}+\sum_{m''\in\mathcal{M}_{\mathcal{R}}\cup\{0\}-\{m'\}}p^R_{m,m'',k,(0)}) +$$

$$\frac{\sum\limits_{m''\in\mathcal{M}_{\mathcal{R}}\cup\{0\}-\{m'\}} p^R_{m,m'',k} - \sum\limits_{m''\in\mathcal{M}_{\mathcal{R}}\cup\{0\}-\{m'\}} p^R_{m,m'',k,(0)}}{(\Psi_{k,m} + \sum\limits_{m''\in\mathcal{M}_{\mathcal{R}}\cup\{0\}-\{m'\}} p^R_{m,m'',k,(0)})\ln(2)}), \tag{56}$$

where $\Psi_{k,m} = \sigma^2_{m,k} + g^{SI}_{k,m}p^{TX}_{k,m}$. The right-hand side in (56) is now concave with respect to $p^{TX}_{k,m'}$.

Furthermore, in the constraint (13d), the term $\sum_{n=1}^{N} a_{n,m'}C_{n,m'}$ is convex with respect to the transmission power over the BS-BS links. However, the term $\sum_{m\in\mathcal{M}_{\mathcal{A}}} C_{m',m}[t]$ is not convex, and the term $C_{0,m'}$ is not concave. Thus, we propose to substitute (13d) with another constraint such that, a fulfillment of the substitute constraint would suffice to fulfill (13d) as well. More specifically, we first derive an under-estimator for the log(.) term in $C_{0,m'}$ according to (12) as follows

$$\log_2(1 + \frac{p^R_{m',0,k}}{\sigma^2_{m',k} + g^{SI}_{k,m'}p^{TX}_{k,m'} + \sum\limits_{m''\in\mathcal{M}_{\mathcal{A}}} p^R_{m,m'',k}}) = \log_2(\sigma^2_{m',k}+$$
$$p^R_{m',0,k} + \chi_{k,m'}) - \log_2(\sigma^2_{m',k} + \chi_{k,m'}) \geq \log_2(\sigma^2_{m',k} + p^R_{m',0,k}+$$
$$\chi_{k,m'}) - \big(\log_2(\sigma^2_{m',k} + \chi_{k,m',(0)}) + \frac{(\chi - \chi_{k,m',(0)})}{(\sigma^2_{m',k} + \chi_{k,m',(0)})\ln(2)}\big), \tag{57}$$

where

$$\chi_{k,m'} = g^{SI}_{k,m'}p^{TX}_{k,m'} + \sum_{m''\in\mathcal{M}_{\mathcal{A}}} p^R_{m,m'',k}, \tag{58}$$

and $\chi_{k,m',(0)}$ is the evaluation of $\chi_{k,m'}$ at the references values $p^{TX}_{k,m',(0)}$ and $p^R_{m,m'',k,(0)}$. The derived lower bound in (57) is now concave with respect to $p^{TX}_{k,m'}$ (note that $p^R_{m,m'',k}$ in (58) is also linearly proportional to $p^{TX}_{k,m'}$ according to (8)), which is the transmission power over the backhaul channels. Note that $p^R_{m,m'',k}$

Next, we propose to derive an over-estimator for $C_{m',m}$. To this end, the log(.) term in (11) is rewritten and upper bounded as follows

$$\log_2(1 + \frac{p^R_{m,m',k}}{\sigma^2_{m,k} + g^{SI}_{k,m}p^{TX}_{k,m} + \sum\limits_{m''\in\mathcal{M}_{\mathcal{R}}\cup\{0\}-\{m'\}} p^R_{m,m'',k}}) =$$

$$\log_2(\sigma^2_{m,k} + g^{SI}_{k,m}p^{TX}_{k,m} + \sum_{m''\in\mathcal{M}_{\mathcal{R}}\cup\{0\}} p^R_{m,m'',k}) - \log_2(\sigma^2_{m,k}+$$

$$g^{SI}_{k,m}p^{TX}_{k,m} + \sum_{m''\in\mathcal{M}_{\mathcal{R}}\cup\{0\}-\{m'\}} p^R_{m,m'',k}) \leq \log_2(\sigma^2_{m,k}+$$
$$g^{SI}_{k,m}p^{TX}_{k,m} + \xi_{m,m',k,(0)}) + \frac{(\xi_{m,m',k} - \xi_{m,m',k,(0)})}{(\sigma^2_{m,k} + g^{SI}_{k,m}p^{TX}_{k,m} + \xi_{m,m',k,(0)})\ln(2)}, \tag{59}$$

where the substitution $\xi_{m,m',k} = \sum\limits_{m''\in\mathcal{M}_{\mathcal{R}}\cup\{0\}-\{m'\}} p^R_{m,m'',k}$ is adopted to avoid cluttering in the presentation of expressions. By adopting the substitutions in (56), (57), and (59), the problem P5** is converted to a convex problem and, therefore, is solved using CVX.

REFERENCES

[1] M. Nikooroo and Z. Becvar, "Optimization of Total Power Consumed by Flying Base Station Serving Mobile Users," in *IEEE Transactions on Network Science and Engineering*, vol. 9, no. 4, pp. 2815-2832, 1 July-Aug. 2022.

[2] W. Chen, W. Xu, L. Lin and C. Huang, "Energy-efficient Cooperative Multi-UAV Coverage Scheme with Limited Wireless Backhaul," *2022 IEEE 22nd International Conference on Communication Technology (ICCT)*, Nanjing, China, 2022, pp. 486-491.

[3] O. Esrafilian, R. Gangula and D. Gesbert, "Learning to Communicate in UAV-Aided Wireless Networks: Map-Based Approaches," in *IEEE Internet of Things Journal*, vol. 6, no. 2, pp. 1791-1802, April 2019.

[4] C. Qiu, Z. Wei, Z. Feng and P. Zhang, "Backhaul-Aware Trajectory Optimization of Fixed-Wing UAV-Mounted Base Station for Continuous Available Wireless Service," in *IEEE Access*, vol. 8, pp. 60940-60950, 2020.

[5] Z. Becvar, M. Nikooroo and P. Mach, "On Energy Consumption of Airship-Based Flying Base Stations Serving Mobile Users," in *IEEE Transactions on Communications*, vol. 70, no. 10, pp. 7006-7022, Oct. 2022.

[6] M. -J. Youssef, J. Farah, C. A. Nour and C. Douillard, "Full-Duplex and Backhaul-Constrained UAV-Enabled Networks Using NOMA," in *IEEE Transactions on Vehicular Technology*, vol. 69, no. 9, pp. 9667-9681, Sept. 2020.

[7] B. Tezergil and E. Onur, "Wireless Backhaul in 5G and Beyond: Issues, Challenges and Opportunities," in *IEEE Communications Surveys & Tutorials*, vol. 24, no. 4, pp. 2579-2632, Fourthquarter 2022.

[8] N. Forouzan, A. M. Rabiei, M. Vehkaperä and R. Wichman, "A Distributed Resource Allocation Scheme for Self-Backhauled Full-Duplex Small Cell Networks," in *IEEE Transactions on Vehicular Technology*, vol. 70, no. 2, pp. 1461-1473, Feb. 2021.

[9] M. Nikooroo, O. Esrafilian, Z. Becvar and D. Gesbert, "Sum Capacity Maximization in Multi-Hop Mobile Networks with Flying Base Stations," *GLOBECOM 2022 - 2022 IEEE Global Communications Conference*, Rio de Janeiro, Brazil, 2022, pp. 6565-6570.

[10] M. Banagar and H. S. Dhillon, "3D Two-Hop Cellular Networks With Wireless Backhauled UAVs: Modeling and Fundamentals," in *IEEE Transactions on Wireless Communications*, vol. 21, no. 8, pp. 6417-6433, Aug. 2022.

[11] T. M. Hoang, L. T. Dung, B. C. Nguyen and T. Kim, "Outage and Throughput Analysis of UAV-Assisted NOMA Relay Systems With Indoor and Outdoor Users," in *IEEE Transactions on Aerospace and Electronic Systems*, vol. 59, no. 3, pp. 2633-2647, June 2023.

[12] M. D. Nguyen, L. B. Le and A. Girard, "UAV Placement and Resource Allocation for Intelligent Reflecting Surface Assisted UAV-Based Wireless Networks," in *IEEE Communications Letters*, vol. 26, no. 5, pp. 1106-1110, May 2022.

[13] Q. -V. Pham, N. Iradukunda, N. H. Tran, W. -J. Hwang and S. -H. Chung, "Joint Placement, Power Control, and Spectrum Allocation for UAV Wireless Backhaul Networks," in *IEEE Networking Letters*, vol. 3, no. 2, pp. 56-60, June 2021.

[14] M. Li, X. Tao, H. Wu and N. Li, "Joint Trajectory and Resource Optimization for Covert Communication in UAV-Enabled Relaying Systems," in *IEEE Transactions on Vehicular Technology*, vol. 72, no. 4, pp. 5518-5523, April 2023.

[15] A. Ahmed, C. Chaieb, W. Ajib, H. Elbiaze and R. Glitho, "Resource Allocation and UAVs Placement in Cell-free Wireless Networks," *GLOBECOM 2022 - 2022 IEEE Global Communications Conference*, Rio de Janeiro, Brazil, 2022, pp. 5995-6000.

[16] X. Ji and T. Wang, "Energy Minimization for Fixed-Wing UAV Assisted Full-Duplex Relaying With Bank Angle Constraint," in *IEEE Wireless Communications Letters*, vol. 12, no. 7, pp. 1199-1203, July 2023.

[17] Y. Yu, X. Bu, K. Yang, H. Yang, X. Gao and Z. Han, "UAV-Aided Low Latency Multi-Access Edge Computing," in *IEEE Transactions on Vehicular Technology*, vol. 70, no. 5, pp. 4955-4967, May 2021.

[18] Y. Liu, W. Huangfu, H. Zhou, H. Zhang, J. Liu and K. Long, "Fair and Energy-Efficient Coverage Optimization for UAV Placement Problem in the Cellular Network," in *IEEE Transactions on Communications*, vol. 70, no. 6, pp. 4222-4235, June 2022.

[19] C. Qiu, Z. Wei, X. Yuan, Z. Feng and P. Zhang, "Multiple UAV-Mounted Base Station Placement and User Association With Joint Fronthaul and Backhaul Optimization," in *IEEE Transactions on Communications*, vol. 68, no. 9, pp. 5864-5877, Sept. 2020.

[20] J. Li et al., "Joint Optimization of Relay Selection and Transmission Scheduling for UAV-Aided mmWave Vehicular Networks," in *IEEE*

Transactions on Vehicular Technology, vol. 72, no. 5, pp. 6322-6334, May 2023.

[21] A. Hajihoseini Gazestani, S. A. Ghorashi, Z. Yang and M. Shikh-Bahaei, "Resource Allocation in Full-Duplex UAV Enabled Multismall Cell Networks," in *IEEE Transactions on Mobile Computing*, vol. 21, no. 3, pp. 1049-1060, 1 March 2022.

[22] P. Mach, Z. Becvar and M. Najla, "Power Allocation, Channel Reuse, and Positioning of Flying Base Stations With Realistic Backhaul," in *IEEE Internet of Things Journal*, vol. 9, no. 3, pp. 1790-1805, 1 Feb.1, 2022.

[23] W. Xu et al., "Throughput Maximization of UAV Networks," in *IEEE/ACM Transactions on Networking*, vol. 30, no. 2, pp. 881-895, April 2022.

[24] T. Liu, M. Cui, G. Zhang, Q. Wu, X. Chu and J. Zhang, "3D Trajectory and Transmit Power Optimization for UAV-Enabled Multi-Link Relaying Systems," in *IEEE Transactions on Green Communications and Networking*, vol. 5, no. 1, pp. 392-405, March 2021.

[25] N. Iradukunda, Q. -V. Pham, M. Zeng, H. -C. Kim and W. -J. Hwang, "UAV-Enabled Wireless Backhaul Networks Using Non-Orthogonal Multiple Access," in *Access*, vol. 9, pp. 36689-36698, 2021.

[26] W. Du, T. Wang, H. Zhang, D. Wu and Y. Li, "Resource Allocation for the Backhaul of NOMA-Based Cellular UAV Network," in *IEEE Transactions on Vehicular Technology*, vol. 71, no. 11, pp. 11889-11899, Nov. 2022.

[27] H. Niu, X. Zhao and J. Li, "3D Location and Resource Allocation Optimization for UAV-Enabled Emergency Networks Under Statistical QoS Constraint," in *IEEE Access*, vol. 9, pp. 41566-41576, 2021.

[28] B. Li, S. Zhao, R. Zhang and L. Yang, "Joint Transmit Power and Trajectory Optimization for Two-Way Multihop UAV Relaying Networks," in *IEEE Internet of Things Journal*, vol. 9, no. 23, pp. 24417-24428, 1 Dec.1, 2022.

[29] S. Seng, C. Luo, X. Li and H. Ji, "Stable Communications in Green Unmanned Aerial Relaying Systems," in *IEEE Internet of Things Journal*, vol. 10, no. 19, pp. 16675-16685, 1 Oct.1, 2023.

[30] D. Yin, X. Yang, H. Yu, S. Chen and C. Wang, "An Air-to-Ground Relay Communication Planning Method for UAVs Swarm Applications," in *IEEE Transactions on Intelligent Vehicles*, vol. 8, no. 4, pp. 2983-2997, April 2023.

[31] N. L. Prasad and B. Ramkumar, "3-D Deployment and Trajectory Planning for Relay Based UAV Assisted Cooperative Communication for Emergency Scenarios Using Dijkstra's Algorithm," in *IEEE Transactions on Vehicular Technology*, vol. 72, no. 4, pp. 5049-5063, April 2023.

[32] M. K. Shehzad, A. Ahmad, S. A. Hassan and H. Jung, "Backhaul-Aware Intelligent Positioning of UAVs and Association of Terrestrial Base Stations for Fronthaul Connectivity," in *IEEE Transactions on Network Science and Engineering*, vol. 8, no. 4, pp. 2742-2755, 1 Oct.-Dec. 2021.

[33] A. Coelho, J. Rodrigues, H. Fontes, R. Campos and M. Ricardo, "An Algorithm for Placing and Allocating Communications Resources Based on Slicing-Aware Flying Access and Backhaul Networks," in *IEEE Access*, vol. 10, pp. 128923-128942, 2022.

[34] S. Yang, D. Shi, Y. Peng, S. Yang, B. Zhang and W. Yang, "Placement Optimization for UAV-Enabled Wireless Networks with Multi-Hop Backhauls in Urban Environments," *2022 21st ACM/IEEE International Conference on Information Processing in Sensor Networks (IPSN)*, Milano, Italy, 2022.

[35] J. Sabzehali, V. K. Shah, Q. Fan, B. Choudhury, L. Liu and J. H. Reed, "Optimizing Number, Placement, and Backhaul Connectivity of Multi-UAV Networks," in *IEEE Internet of Things Journal*, vol. 9, no. 21, pp. 21548-21560, 1 Nov.1, 2022.

[36] L. -C. Wang, Y. -S. Chao, S. -H. Cheng and Z. Han, "An Integrated Affinity Propagation and Machine Learning Approach for Interference Management in Drone Base Stations," in *IEEE Transactions on Cognitive Communications and Networking*, vol. 6, no. 1, pp. 83-94, March 2020.

[37] M. Nikooroo, Z. Becvar, O. Esrafilian and D. Gesbert, "QoS-Aware Sum Capacity Maximization for Mobile Internet of Things Devices Served by UAVs," *2022 IEEE 33rd Annual International Symposium on Personal, Indoor and Mobile Radio Communications (PIMRC)*, Kyoto, Japan, 2022, pp. 1-7.

[38] M. Nikooroo, Z. Becvar, O. Esrafilian and D. Gesbert, "Channel Reuse for Backhaul in UAV Mobile Networks with User QoS Guarantee," *ICC 2023 - IEEE International Conference on Communications*, Rome, Italy, 2023, pp. 5425-5431.

[39] B. Li, Q. Li, Y. Zeng, Y. Rong and R. Zhang, "3D Trajectory Optimization for Energy-Efficient UAV Communication: A Control Design Perspective," in *IEEE Transactions on Wireless Communications*, vol. 21, no. 6, pp. 4579-4593, June 2022.

[40] H. Wang, J. Wang, G. Ding, J. Chen, Y. Li and Z. Han, "Spectrum Sharing Planning for Full-Duplex UAV Relaying Systems With Underlaid D2D Communications," in *IEEE Journal on Selected Areas in Communications*, vol. 36, no. 9, pp. 1986-1999, Sept. 2018.

[41] S. Wright, "Primal-Dual Interior-Point Methods," Society for Industrial and Applied Mathematics, 1997.

[42] MB Cohen, et al, "Solving linear programs in the current matrix multiplication time." Journal of the ACM (JACM) 68.1 (2021): 1-39.

[43] J. Lee and V. Friderikos, "Trajectory Planning for Multiple UAVs in UAV-aided Wireless Relay Network," *ICC 2022 - IEEE International Conference on Communications*, Seoul, Korea, Republic of, 2022, pp. 1-6.

[44] L. He, R. Chai and R. Sun, "Cost Efficient UAV Deployment and Resource Allocation for UAV-Assisted Networks," *2022 IEEE 96th Vehicular Technology Conference (VTC2022-Fall)*, London, United Kingdom, 2022, pp. 1-5.

[45] S. E. Sabino and A. M. Grilo, "NSGA-II Based Joint Topology and Routing Optimization of Flying Backhaul Networks," in *IEEE Access*, vol. 10, pp. 96180-96196, 2022.

[46] M. Nikooroo and Z. Becvar, "Optimal Positioning of Flying Base Stations and Transmission Power Allocation in NOMA Networks," in *IEEE Transactions on Wireless Communications*, vol. 21, no. 2, pp. 1319-1334, Feb. 2022.

[47] R. C. DiPietro, "An FFT based technique for suppressing narrow-band interference in PN spread spectrum communications systems," *International Conference on Acoustics, Speech, and Signal Processing,* Glasgow, UK, 1989, pp. 1360-1363 vol.2.

[48] A. A. Baba, R. M. Hashmi and K. P. Esselle, "Achieving a Large Gain-Bandwidth Product From a Compact Antenna," in *IEEE Transactions on Antennas and Propagation*, vol. 65, no. 7, pp. 3437-3446, July 2017.

[49] M. Nikooroo and Z. Becvar, "Optimization of Transmission Power for NOMA in Networks with Flying Base Stations," *2020 IEEE 92nd Vehicular Technology Conference (VTC2020-Fall)*, Victoria, BC, Canada, 2020, pp. 1-7.

[50] K. Liu and J. Zheng, "UAV Trajectory Optimization for Time-Constrained Data Collection in UAV-Enabled Environmental Monitoring Systems," in *IEEE Internet of Things Journal*, vol. 9, no. 23, pp. 24300-24314, 1 Dec.1, 2022.

[51] R. Chen, Y. Sun, L. Liang and W. Cheng, "Joint Power Allocation and Placement Scheme for UAV-Assisted IoT With QoS Guarantee," in *IEEE Transactions on Vehicular Technology*, vol. 71, no. 1, pp. 1066-1071, Jan. 2022.